Gas Injection Optimization under Uncertainty in Subsurface Reservoirs: An Integrated Machine Learning Assisted Workflow

Xupeng He, Dr. Hussain Hoteit, Marwah M. AlSinan and Dr. Hyung T. Kwak

Abstract /

Gas injection in subsurface reservoirs is of significant interest to the petroleum industry for the enhanced oil recovery (EOR) process. There exists geological uncertainty in the subsurface due to the limited measurements. Optimization under such uncertainty is, therefore, required to make more robust operational decisions to achieve maximum EOR with a minimum risk of early breakthrough.

This work introduces an integrated machine learning assisted workflow for the optimization under uncertainty in subsurface reservoirs. The proposed workflow includes three steps: (1) Training sample generation. We first identify the uncertain parameters, which affect the objective of interests. We then generate the input designs using Latin Hypercube Sampling (LHS) based on the identified uncertain parameters. High fidelity simulations based on the MATLAB Reservoir Simulation Toolbox (MRST) are run for each of the input designs to obtain the objective of interests as outputs. (2) Surrogate model development. A data-driven surrogate model is then built to model the nonlinear mapping between the input and output results from Step 1. Herein, the Bayesian optimization technique is implemented to obtain the surrogate model. (3) Optimization under uncertainty. We first conduct a blind test on the proposed surrogate model with high fidelity simulations. Followed by Monte Carlo to perform the uncertainty quantifications and a genetic algorithm (GA) to conduct the optimization.

This work introduces an efficient, robust, and accurate machine learning assisted workflow for gas injection optimization under uncertainty in subsurface reservoirs. To our best knowledge, this approach is applied for the first time.

Introduction

Subsurface reservoirs exhibit geological uncertainty since we have a limited number of measurements. Such uncertainty can make the decision making process very challenging. Gas injection problems often feature more complex physics because of the significant contrast in compressibility and density compared to water injection cases. This work takes gas injection into oil reservoirs as an example, and introduces an efficient and robust workflow for optimization under uncertainty using machine learning techniques.

Recent advances in machine learning have inspired many applications in the petroleum industry. Examples include fracture recognition from outcrops, upscaling of discrete fracture models, fracture permeability estimation, multicomponent flash calculation, and carbon dioxide leakage rate forecasting[1-6]. Their studies demonstrate that provided with large amounts of high quality data sets and optimal network hyperparameters, this technology is competitive to traditional approaches in terms of accuracy and efficiency.

The abovementioned applications correspond to four network architectures, respectively: (1) U-Net for image-to-image problems, (2) convolutional neural network for image to value problems, (3) artificial neural network (ANN) for value-to-value problems, (4) long short-term memory (LSTM) for time series problems. The ANN model, with time as input also could deal with time series problems, yet honors simplicity and efficiency compared to LSTM[7, 8]. In this work, the surrogate model developed by ANN will replace the expensive high fidelity simulation model.

The proposed workflow is comprised of three steps: (1) training sample generation, (2) surrogate model development, and (3) optimization under uncertainty.

Problem Statement

We consider injecting gas into oil reservoirs as an example. The continuity equation and Darcy's law are applied to govern the corresponding physics, in which the continuity equation of phase, α, is expressed as:

$$\frac{\partial(\phi\rho_\alpha S_\alpha)}{\partial t} + \nabla\cdot\left(\rho_\alpha \overline{u_\alpha}\right) = Q_\alpha \qquad \alpha = g, o \tag{1}$$

where Q is the sink/source term, $\overline{u}$ is velocity, p is density, S is saturation, ϕ is porosity, and t is time.

Darcy's law models the velocity as:

$$\overline{u_\alpha} = -\frac{k_{r\alpha}}{\mu_\alpha}\vec{K}\left(\nabla p_\alpha + \rho_\alpha g \nabla z\right) \quad (2)$$

where k_r is the relative permeability, μ is viscosity, $\vec{K}$ is the absolute permeability tensor, p is pressure, g is gravity acceleration, and z is the depth. We constrain phase saturations by using the following equation:

$$S_g + S_o = 1 \quad (3)$$

and relate two pressures by capillary pressure (denoted by P_c) function:

$$P_c(S_w) = P_g - P_o \quad (4)$$

The time-dependent oil recovery factor (denoted by RF_o), as one objective of interest, is given by:

$$RF_o(t) = \frac{\left(\int_0^t Q_p dt\right) \cdot B_o}{Vb \cdot \phi \cdot S_{o_{ini}}} \quad (5)$$

where Q_p is production rate measured under standard conditions, B_o is the oil formation volume factor, Vb is the bulk reservoir volume, and $S_{o_{ini}}$ is the initial oil saturation. The other objective of interest refers to the time when gas breakthrough occurs (denoted by t_{break}).

We implement the first Society of Petroleum Engineers benchmark as the high fidelity simulation model. It is a live oil/dry gas black oil model with nearly immobile water. The model is initially undersaturated with a uniform mixture of water ($S_{w_{ini}}$ = 0.12) and oil ($S_{o_{ini}}$ = 0.88) with no initial free gas ($S_{g_{ini}}$ = 0). We assume a constant dissolved gas-oil ratio throughout the model. The model resembles a three-layer cake configuration, in which each layer is assumed to be homogeneous and isotropic. Future work will address significantly heterogeneous and anisotropic cases. The geological uncertainty is represented by changing the permeability value and corresponding porosity value for each layer. In this study, the high fidelity simulation is solved by a fully implicit black oil solver within the MATLAB Reservoir Simulation Toolbox (MRST) framework. A detailed numerical implementation can be found in Lie (2019)[9].

We consider a base case, in which permeability values of 2,000 mD, 200 mD, and 800 mD are assigned to each layer with a constant gas injection rate of 100 million standard cubic feet per day (MMscfd). The oil production rate is fixed before breakthrough and then converts to constant borehole pressure, i.e., bottom-hole pressure, after breakthrough. Other parameters and their corresponding values are provided in Lie (2019)[9] and Odeh (1981)[10].

Figure 1 illustrates the layered cake permeability distribution and diagonally opposite well placement. Figure 2 shows the gas saturation with the increasing time for the base case.

Proposed Workflow

Although the high fidelity simulation model provides the most accurate methodology for capturing the physics, it suffers from intensive computation costs. Multiple simulation runs are required for applications such as optimization under uncertainty, making it infeasible for practical engineering purposes, e.g., quick decision making. It integrates knowledge of sampling techniques, machine learning, uncertainty quantification, and multi-object optimization.

We will detail the workflow in the following three steps, Fig. 3.

Training Sample Generation

We first identify the uncertain parameters that impact the objective of interests, i.e., EOR and breakthrough time. With these identified uncertain parameters, various input designs are generated using Latin Hypercube Sampling (LHS). The implementation of LHS guarantees data samples are distributed in a space filling manner

Fig. 1 The layered cake permeability distribution and well placement.

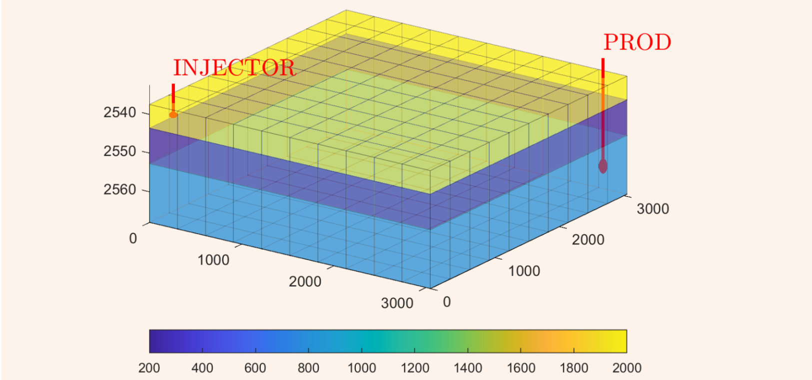

Fig. 2 The gas saturation with increasing time. We observe the typically gravity dominated flow behavior, i.e., gas tending to migrate upwards, due to the significant contrast in density between the gas and oil.

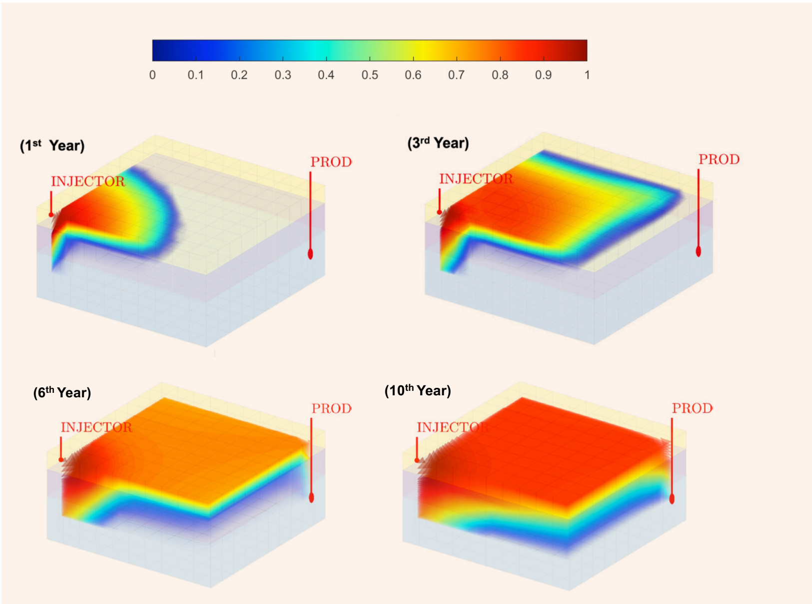

Fig. 3 *The proposed workflow includes three steps: (1) training sample generation, (2) surrogate model development, and (3) optimization under uncertainty.*

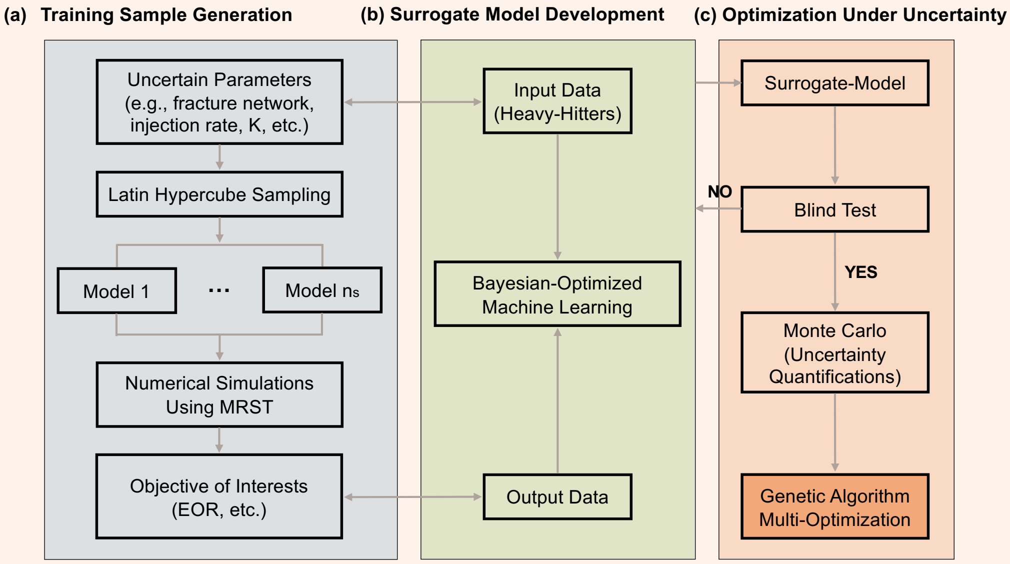

instead of a clustering manner[2, 3, 11].

Table 1 summarizes the identified uncertain parameters, including geological and operational (in light blue). Their corresponding ranges are collected from the literature, in which range of permeability is adopted and modified from the North Sea fields[12]. Correlation between porosity and permeability is modified from Chen and Pawar (2019)[7], in which we reduce the exponential coefficient to account for a bigger range of permeability values. The range of gas injection rates are collected from various projects in the North Sea, and example cases from MRST[9, 13]. We assume all uncertain parameters to be independent with uniform distributions except for porosity. The corresponding values of porosity are calculated based on permeability values using the correlation in Table 1. (Note: K_1, K_2, and K_3 correspond to permeability values of the first, second, and third layer, respectively.)

High fidelity simulations based on MRST[9] are run for each input design to generate the corresponding objective of interests as output. We then collect the inputs and outputs to be read for training the surrogate model.

Surrogate Model Development

This step strives to build a data-driven, physics featuring surrogate model to map the nonlinear relation between the inputs and outputs obtained earlier. Figure 4 shows the implemented ANN architecture with one input layer, various hidden layers, one output layer. The time term (in red) is added into the input layer to capture time-dependent problems. Three key elements, including the ratio of training to validation samples, proper network architecture, and optimal weights and biases, are critical for obtaining a successfully surrogate ANN model. Obviously, choosing appropriate hyperparameters related to these three elements is challenging.

The traditional approach of tuning hyperparameters based on trial and error is exhaustive and labor intensive. As an alternative, Bayesian optimization is implemented to automate the tuning process in this work. A detailed description of Bayesian optimization could be found in Frazier (2018)[14].

Table 1 *The identified uncertain parameters and corresponding ranges and distributions.*

Uncertain Parameters	Lower Bound	Upper Bound	Distribution
Permeability (K_1)	200 mD	2,000 mD	Uniform
Permeability (K_2)	200 mD	2,000 mD	Uniform
Permeability (K_3)	200 mD	2,000 mD	Uniform
Porosity ($\emptyset$)	0.24	0.375	$\emptyset = 0.082 \times K^{0.2}$
Gas Injection Rate (Q_{inj})	80 MMscfd	134 MMscfd	Uniform

Fig. 4 The implemented ANN architecture with one input layer, various hidden layers, and one output layer.

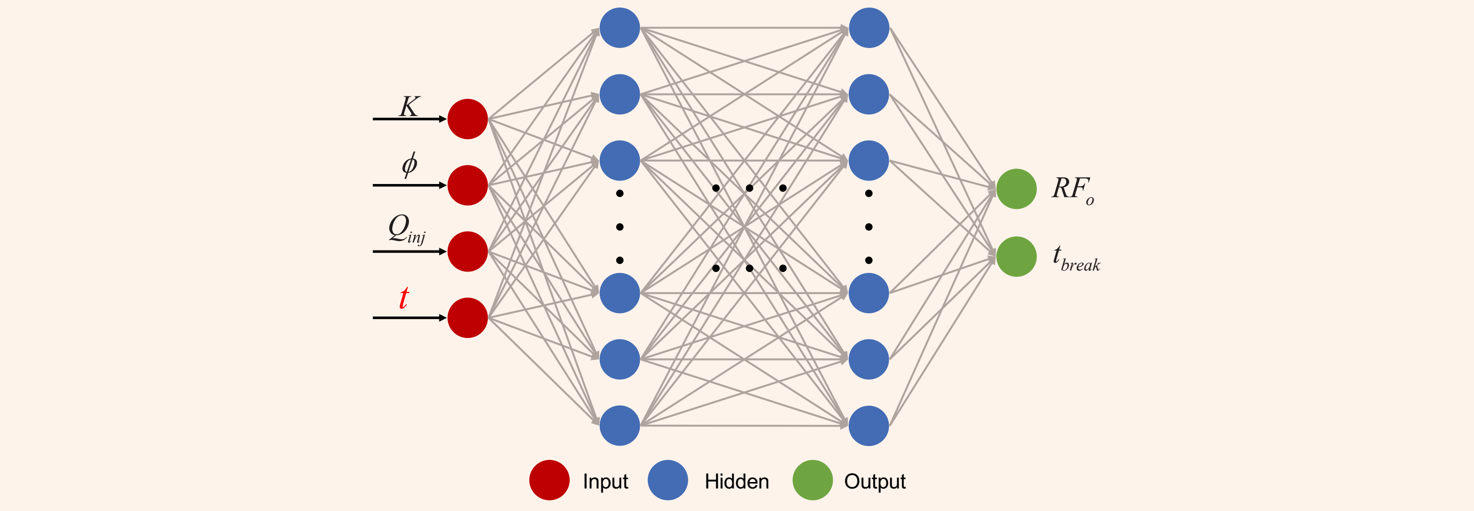

Attention should be paid to the coupled training validation process regarding overfitting and gradient vanishing issues. The overfitting issue takes place with a considerable number of epochs. The gradient vanishing issue occurs when choosing deep neural networks.

Optimization under Uncertainty

In this step, we perform gas injection optimization under these geological uncertainties to achieve maximum EOR while maintaining the minimum risk of early breakthrough.

We further validate the developed surrogate model using various blind cases. The following parameters are used to evaluate its performance.

- APE: The average of prediction errors (PE) between the predicted (denoted by M^P) and ground truth (denoted by M^G) solutions. M refers to the objective of interests, i.e., recovery factor or gas breakthrough time.

$$PE = \left|\frac{M^P - M^G}{M^G}\right| \times 100\% \qquad (6)$$

$$APE = \frac{1}{N}\sum_{i=1}^{N} PE_i \qquad (7)$$

- PPE: The percentage of PEs within an acceptable error margin — herein, 10%.

$$PPE = \frac{N_{(where, PE \le 10\%)}}{N} \times 100\% \qquad (8)$$

- RMSE: The root-mean-square error of PEs.

$$RMSE = \sqrt{\frac{\sum_{i=1}^{N} PE_i^2}{N}} \qquad (9)$$

where N is the total number of points.

If values of these three parameters are within certain ranges, it means the developed surrogate model passes the blind test and could be implemented as a fully trusted surrogate. Otherwise, we need to retrain the ANN model by increasing the number of samples or adjusting the ratio of training to validation samples. This process is repeated until the trained surrogate model passes the blind test.

We then perform Monte Carlo simulations based on the fully trusted surrogate model to explore uncertainty propagation behaviors. The corresponding responses are grouped in the way from which the probabilistic forecast of percentiles, P_{10}, P_{50}, and P_{90}, are quantified. We increase the number of runs until P_{10}, P_{50}, and P_{90} values tend to be stable. The uncertain ranges provide a rough estimation of the objective of interests under the ranges of uncertain parameters, previously listed in Table 1.

In this work, the genetic algorithm (GA) is performed to a multi-object optimization problem — maximum EOR while minimum risk of breakthrough — to determine the optimized gas injection rate. We then deploy the Pareto front to seek a compromise between the oil recovery factor and gas breakthrough time.

The key to the proposed workflow is guaranteeing a fully trusted surrogate model. More rigorous measures are therefore required to assure the robustness of the proposed workflow.

Results and Discussion

Following the first two steps previously discussed, we generate 50 input designs based on LHS and run the high fidelity simulations using MRST. We select 20 time steps from each simulation and have a total of 1,000 data samples for the Bayesian optimized training validation process. Table 2 summarizes the optimal ratio of training to validation samples, the Bayesian optimized ANN architecture and hyperparameters, and model evaluation performance. For illustration purposes, we only show oil recovery as an example. Gas breakthrough time follows

Table 2 *The optimized ANN architecture, ANN hyperparameters, and model performance.*

ANN Architecture and Hyperparameters	Four hidden layers with 4, 7, 8, and 6 neurons, respectively.	
Model Training	Training Samples	700 (70%)
	APE	1.7%
	PPE	97%
	RMSE	4.4%
Model Validation	Validation Samples	300 (30%)
	APE	1.4%
	PPE	99%
	RMSE	3.5%

the same way and will not be detailed.

As observed in Table 2, the Bayesian optimized ANN architecture features four hidden layers with 4, 7, 8, and 6 neurons on each layer. The optimal ratio of training to validation samples is 7:3. The optimized model achieves accuracy exceeding 95% on both the training and validation samples with PPE of 97% and 99%, respectively.

Overfitting issues typically occur — good predictions, i.e., small errors, on training data, yet poor performance for validation samples, Fig. 5. The model performance in terms of validation shows an optimum epoch, before and after which two statuses are underfitting and overfitting, respectively.

Another issue we need to pay attention to is the gradient vanishing issue, as weight and biases will not be updated with a very long network structure. According to the chain rule, the gradient term (highlight in blue) in Eqn. 10 is the multiplication of many derivative terms. If with very deep neural networks, the blue term is almost zero, which leads to weights not being updated. Therefore, proper network architecture is also crucial for obtaining a successfully trained model.

$$W_{new} = W_{old} - \eta \bullet \frac{\partial Loss}{\partial W} \quad (10)$$

Figures 6a and 6b illustrates the diagonal plots between

Fig. 5 *The epoch vs. MSE of the model.*

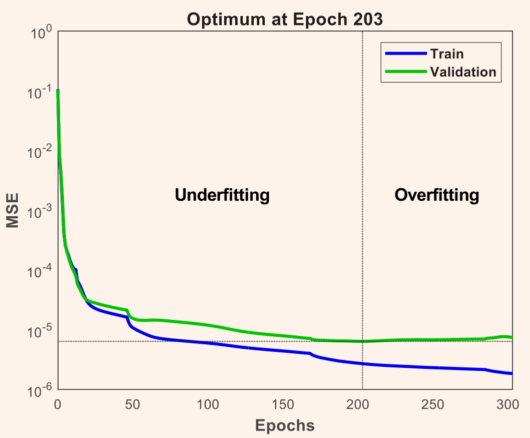

Fig. 6 *The diagonal plots showing the surrogate vs. ground truth predictions for (a) training, and (b) validation samples.*

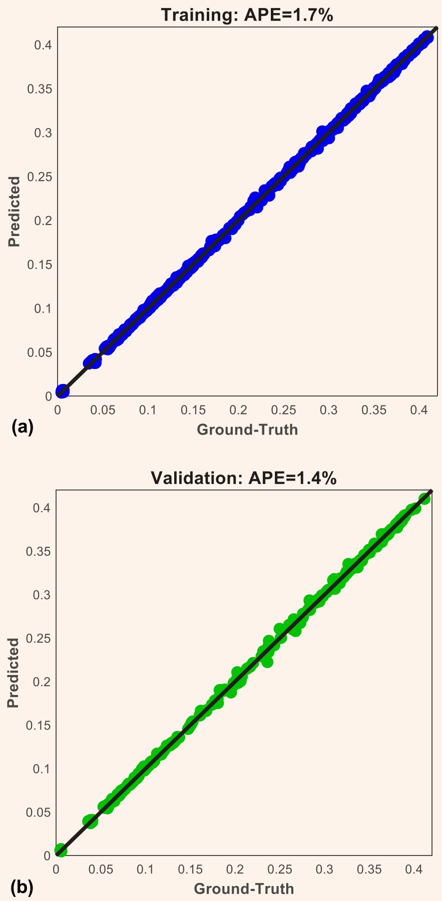

the trained surrogate and ground truth solutions, respectively. Datapoints falling on the diagonal line means an exact match, while in off-diagonal regions shows deviations. As shown, the off-diagonal points are almost equally distributed on both sides of the diagonal line, indicating the surrogate model shows stable performance instead of all overestimation or underestimation situations. The APEs on training and validation samples are 1.7% and 1.4%, respectively.

The key to the proposed workflow is guaranteeing a fully trusted surrogate model. Blind tests with four newly generated cases are selected further to verify the accuracy of the optimized surrogate model, plotted in the form of oil recovery vs. time, Fig. 7. Results show an excellent match with the ground truth solutions, meaning the developed surrogate model could be treated as a fully trusted model for future applications.

We then conduct 5,000 Monte Carlo runs to explore the uncertainty propagation behaviors using the fully trusted surrogate model, which are proven to be stable in terms of the values of P_{10}, P_{50}, and P_{90}. The uncertain ranges provide a rough estimation of variation of oil recovery under the ranges of uncertain parameters in Table 1.

Figure 8 illustrates the uncertainty analysis for time series oil recovery based on the 5,000 runs. We observe three prominent trends; recovery factors increase gradually with a very narrow range at the early stage, then increase abruptly in the middle stage, and finally reach a stable trend. Yet, recovery factors show a wide uncertainty range in the last two stages. These three trends reflect three corresponding physical processes: (1) before the gas breakthrough (only oil production stage), (2) early-stage gas breakthrough (low gas-oil ratio stage), and (3) later gas breakthrough (high gas-oil ratio stage).

Fig. 8 *Uncertainty analysis for time-dependent oil recovery factor based on 5,000 Monte Carlo runs applied to the fully trusted surrogate model.*

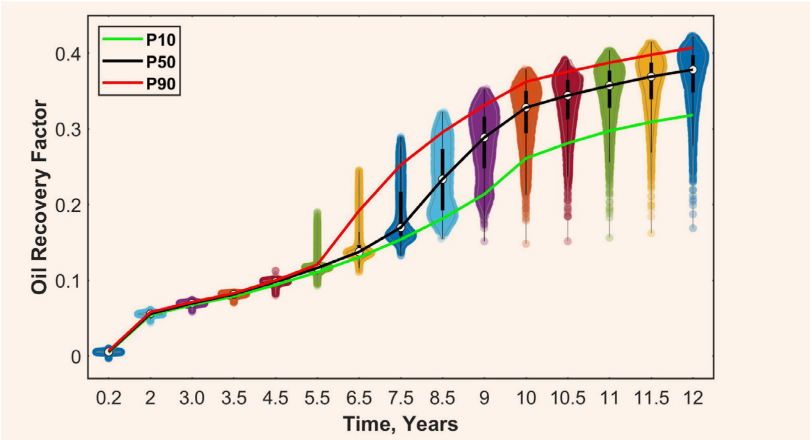

Fig. 7 *The blind test with four new cases between the proposed surrogate and ground truth predictions, showing a good match.*

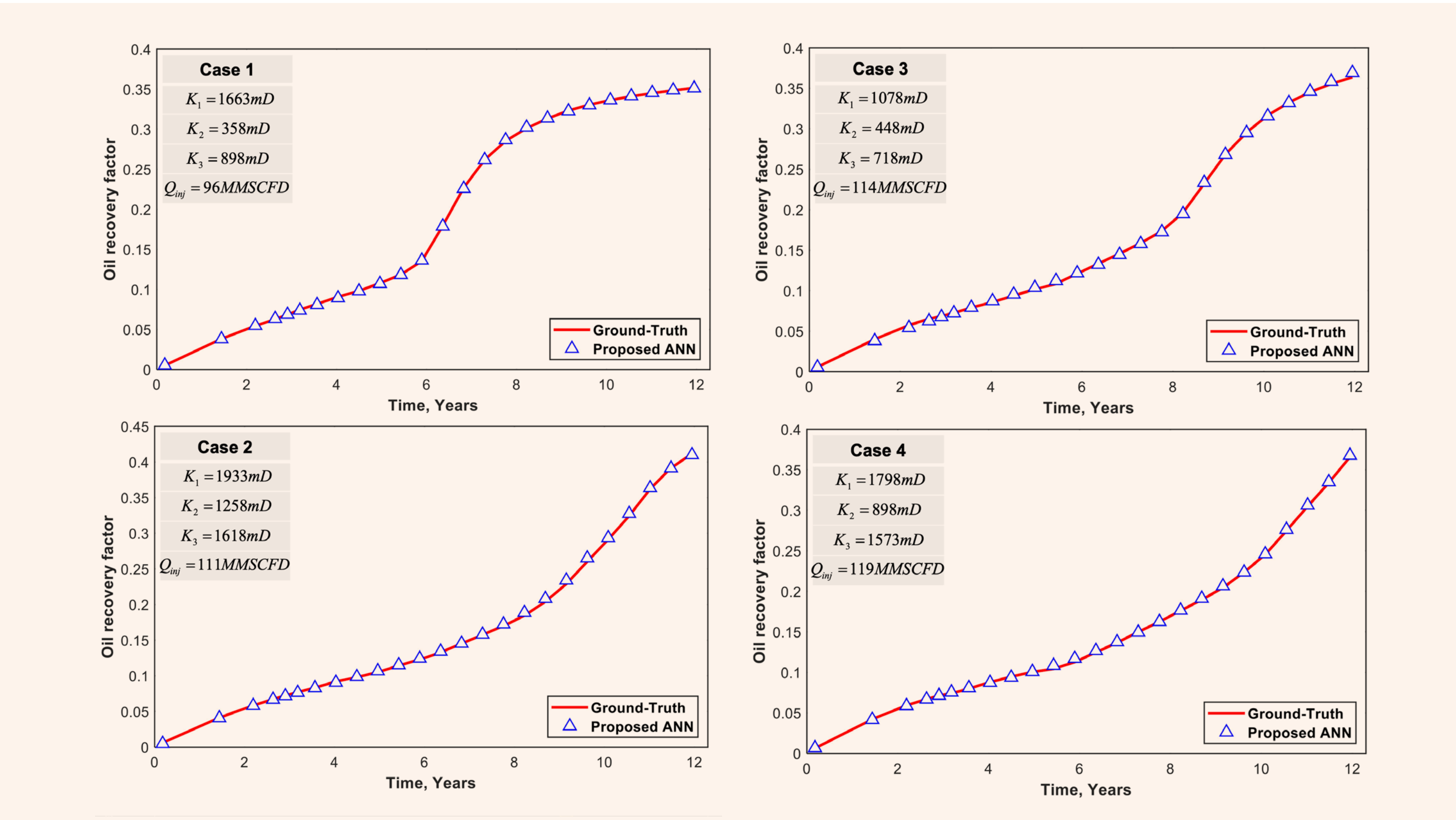

Fig. 9 The gas breakthrough time vs. oil recovery at breakthrough (blue squares) and final time (red stars).

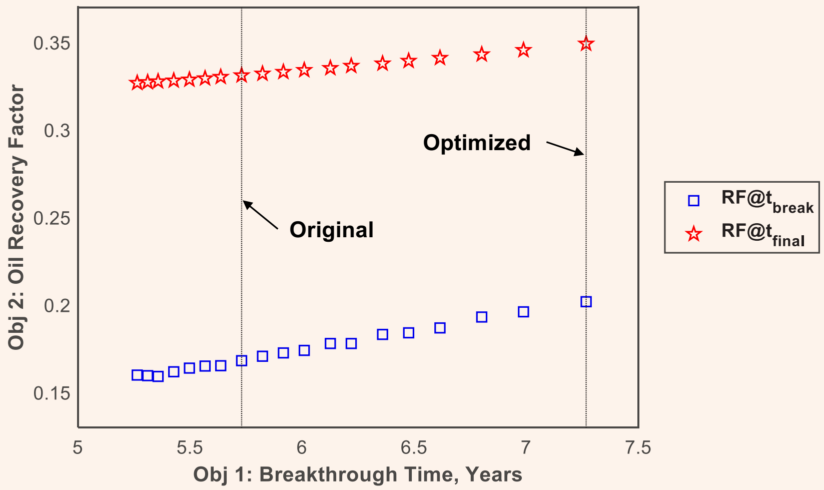

We finally perform optimization to achieve the best recovery factor with a minimum risk of gas breakthrough, belonging to the constrained multi-objective optimization problem. We only have gas injection rate as the decision variable. The Pareto front is plotted to seek a compromise between the oil recovery factor and gas breakthrough time. For illustration purposes, we take the base case as an example with varying gas injection rates.

Figure 9 shows the relation between two objectives; gas breakthrough vs. oil recovery at breakthrough and final time. We obtain an optimized gas injection rate of 134 MMscfd, under which we have the maximum oil recovery at both states — 0.20 and 0.35 — and the longest non-gas breakthrough production time of 7.3 years.

Conclusions

This work introduces an efficient, robust, and accurate machine learning assisted workflow designed for gas injection optimization under geological uncertainty to achieve maximum EOR with a minimum risk of early breakthrough. It incorporates knowledge of sampling techniques, machine learning, uncertainty quantification, and multi-object optimization. To our best knowledge, this approach is implemented for the first time. We summarize the main findings as.

1. An ANN with time term as input could capture time-dependent problems (oil recovery vs. time), yet honoring more simplicity and flexibility than the LSTM.
2. The implementation of LHS assures space filling data samples. The data samples generally show clustering distribution without the guidance of LHS, which results in unbalanced performance, i.e., good performance on samples from the clustered area, but poor predictions on samples from the sparse area.
3. The quality of samples significantly impacts the quality of the surrogate model and furthers its predictability. Herein, high fidelity simulations using a fully implicit black oil solver within the MRST are applied to generate the training and validation samples.
4. For the fixed number of data samples, optimal hyperparameters — including network structure — are crucial for obtaining a successful ANN-based surrogate model. Herein, we employ Bayesian optimization to automate the process of tuning hyperparameters instead of traditional trial error.
5. Special attention should be paid to overfitting and gradient vanishing issues during the coupled training validation process. An optimal epoch is selected to avoid overfitting issues. A proper number of hidden layers is chosen to prevent vanishing gradient issues.
6. A blind test is required to verify the accuracy of the trained model further to obtain a fully trusted surrogate model. More rigorous measures are needed, such as increasing the number of data samples or adjusting the ratio of training to validation samples.
7. Monte Carlo runs based on the fully trusted surrogate model are performed to explore the uncertainty propagation behaviors. We should assure stable and convergent results by increasing the number of runs.
8. A GA is performed to optimize the operational parameter, i.e., gas injection rate, to achieve maximum EOR with a minimum risk of early breakthrough — multi-object optimization problems. The Pareto front is employed to seek a compromise between the oil recovery factor and gas breakthrough time.
9. The proposed workflow shows great potential for optimization under uncertainty and could be extended to more general applications, such as in fractured reservoirs or coupled with history matching workflow.

Future work will focus on exploring the performance in terms of accuracy and efficiency between ANN and

LSTM in describing complex time-dependent problems. Also, more complex cases should be addressed, such as significant heterogeneous cases.

Acknowledgments

The authors would like to thank Saudi Aramco for funding this research. We would also like to thank King Abdullah University of Science and Technology (KAUST) for providing the licenses of MATLAB.

Additional Information

Any discussion on this article is highly encouraged. All codes are developed in a MATLAB environment and are available upon request (xupeng.he@kaust.edu.sa). Citing the article is required once implementing the original or modified codes.

References

1. He, X., Santoso, R. and Hoteit, H.: "Application of Machine Learning to Construct Equivalent Continuum Models from High-Resolution Discrete Fracture Models," IPTC paper 20040, presented at the International Petroleum Technology Conference, Dhahran, Kingdom of Saudi Arabia, January 13-15, 2020.

2. He, X., Zhu, W., Santoso, R., AlSinan, M.M., et al.: "CO_2 Leakage Rate Forecasting Using Optimized Deep Learning," SPE paper 206222, presented at the SPE Annual Technical Conference and Exhibition, Dubai, UAE, September 21-23, 2021.

3. He, X., Zhu, W., Santoso, R., AlSinan, M.M., et al.: "Fracture Permeability Estimation under Complex Physics: A Data-Driven Model Using Machine Learning," SPE paper 206352, presented at the SPE Annual Technical Conference and Exhibition, Dubai, UAE, September 21-23, 2021.

4. Li, Y., Zhang, T. and Sun, S.: "Acceleration of the NVT Flash Calculation for Multicomponent Mixtures Using Deep Neural Network Models," *Industrial & Engineering Chemistry Research*, Vol. 58, Issue 27, 2019, pp. 12312-12322.

5. Santoso, R., He, X. and Hoteit, H.: "Application of Machine Learning to Construct Simulation Models from High-Resolution Fractured Formation," SPE paper 197439, presented at the Abu Dhabi International Petroleum Exhibition and Conference, Abu Dhabi, UAE, November 11-14, 2019.

6. Zhang, T., Li, Y., Li, Y., Sun, S., et al.: "A Self-Adaptive Deep Learning Algorithm for Accelerating Multicomponent Flash Calculation," *Computer Methods in Applied Mechanics and Engineering*, Vol. 369, September 2020.

7. Chen, B. and Pawar, R.J.: "Characterization of CO_2 Storage and Enhanced Oil Recovery in Residual Oil Zones," *Energy*, Vol. 183, September 2019, pp. 291-304.

8. Kim, Y., Jang, H., Kim, J. and Lee, J.: "Prediction of Storage Efficiency on CO_2 Sequestration in Deep Saline Aquifers Using Artificial Neural Network," *Applied Energy*, Vol. 185, Issue 1, January 2017, pp. 916-928.

9. Lie, K-A.: *An Introduction to Reservoir Simulation Using MATLAB/GNU Octave: User Guide for the MATLAB Reservoir Simulation Toolbox (MRST)*, Cambridge University Press, 2019, 677 p.

10. Odeh, A.S.: "Comparison of Solutions to a Three-Dimensional Black Oil Reservoir Simulation Problem," includes associated paper 9741, *Journal of Petroleum Technology*, Vol. 33, Issue 1, January 1981, pp. 13-25.

11. Santoso, R., Hoteit, H. and Vahrenkamp, V.: "Optimization of Energy Recovery from Geothermal Reservoirs Undergoing Re-injection: Conceptual Application in Saudi Arabia," SPE paper 195155, presented at the SPE Middle East Oil and Gas Show and Conference, Manama, Kingdom of Bahrain, March 18-21, 2019.

12. Teigland, R. and Kleppe, J.: "EOR Survey in the North Sea," SPE paper 99546, presented at the SPE/DOE Symposium on Improved Oil Recovery, Tulsa, Oklahoma, April 22-26, 2006.

13. Cavanagh, A. and Ringrose, P.: "Improving Oil Recovery and Enabling CCS: A Comparison of Offshore Gas Recycling in Europe to CCUS in North America," *Energy Procedia*, Vol. 63, 2014, pp. 7677-7684.

14. Frazier, P.I.: "A Tutorial on Bayesian Optimization," *arXiv:1807.02811*, 2018.

About the Authors

Xupeng He

M.S. in Petroleum Engineering, King Abdullah University of Science and Technology

Xupeng He is currently a Ph.D. student at the Ali I. Al-Naimi Petroleum Engineering Research Center, King Abdullah University of Science and Technology (KAUST), Thuwal, Saudi Arabia. His research interests include modeling naturally fractured reservoirs, machine (deep) learning applications in petroleum engineering, and uncertainty quantification and optimization in subsurface flow problems.

Xupeng is the author of 11 conference papers, and two U.S. patents.

He was the recipient of the Excellent Student Cadre and the Outstanding Undergraduate Student Awards in 2014 and 2015, respectively, at Chang'an University. Also, Xupeng received a national scholarship from the Ministry of Education of the People's Republic of China in 2012 and 2013.

He received his B.S. degree in Resource Exploration Engineering (Oil and Gas) from Chang'an University, Xi'an, China, in 2015. Xupeng received his M.S. degree in Petroleum Engineering from KAUST in 2018.

Dr. Hussein Hoteit

Ph.D. in Applied Mathematics, University of Rennes 1

Dr. Hussein Hoteit is an Associate Professor in Reservoir Engineering and the Program Chair of Energy Resources and Petroleum Engineering (ERPE) at King Abdullah University of Science and Technology (KAUST), Thuwal, Saudi Arabia.

Before joining KAUST, Hussein worked for ConocoPhillips and Chevron Companies for about 12 years, where he conducted projects related to chemical enhanced oil recovery (EOR), CO_2 EOR, steam flood, EM heating, to name a few.

Hussein's current research includes chemical EOR, geological CO_2 storage, improved oil recovery optimization, data-driven machine learning, and reservoir simulation development.

He has earned several Society of Petroleum Engineers (SPE) awards, including SPE Distinguished Lecturer in 2009, and served as Associate Editor for the *SPE Journal* for more than 10 years.

Hussein received his B.S. degree in Pure Mathematics and Computer Sciences from Lebanese University, Lebanon, M.S. and Ph.D. degrees in Applied Mathematics from the University of Rennes 1, Rennes, France.

Marwah M. AlSinan

M.S. in Petroleum Engineering, Imperial College

Marwah M. AlSinan joined Saudi Aramco in 2013 as a Petroleum Engineer, working with the Reservoir Engineering Technology Division in the Exploration and Petroleum Engineering Center – Advanced Research Center (EXPEC ARC).

Her research interests include multiphase flow in fractures, carbon dioxide sequestration, and applications of nuclear magnetic resonance in porous media.

In 2013, Marwah received her B.S. degree in Petroleum and Natural Gas Engineering from Pennsylvania State University, State College, PA. She received her M.S. degree in Petroleum Engineering from Imperial College, London, U.K. in 2017.

Dr. Hyung T. Kwak

Ph.D. in Physical Chemistry, Ohio State University

Dr. Hyung T. Kwak joined Saudi Aramco in April 2010 as a Petroleum Engineer with Saudi Aramco's Exploration and Petroleum Engineering Center – Advanced Research Center (EXPEC ARC). He had been a member of the Pore Scale Physics focus area and the SmartWater Flooding focus area of the Reservoir Engineering Technology Division. Since 2014, Hyung has been a focus area champion of the Pore Scale Physics focus area. His main research focus is seeking a deeper understanding of fluid-rock interaction in pore scale of the Kingdom's reservoirs.

Since joining Saudi Aramco, Hyung has been involved with various improved oil recovery and enhanced oil recovery (EOR) research projects, such as SmartWater Flooding, carbon dioxide EOR, and chemical EOR. Currently, he is leading a suite of key EXPEC ARC Fourth Industrial Revolution technology projects. Prior to joining Saudi Aramco, Hyung was a Research Scientist at Baker Hughes, from 2001 to 2010, focused on research related to nuclear magnetic resonance (NMR)/magnetic resonance imaging technology.

In 1996, Hyung received his B.S. degree in Chemistry from the University of Pittsburgh, Pittsburgh, PA, and in 2001, he received his Ph.D. degree in Physical Chemistry from Ohio State University, Columbus, OH.

Before moving into the oil and gas industry, Hyung was involved — as a postdoctoral fellow for 2 years — in a project developing the world's largest wide bore superconducting magnet NMR spectrometer, 900 MHz, at the National High Magnetic Field Laboratory.

He has more than 300 publications, including peer-reviewed articles and patents.

Graphene Modified with Linear Alkylamines for Oil Pollutants Removal from Water

Norah W. Aljuryyed and Fahd I. Alghunaimi

Abstract / Three stable and robust types of graphene, modified with linear alkylamines, including n-propylamine, n-hexylamine, and n-dodecylamine, were synthesized. The prepared materials, graphene modified with n-propylamine (GPA), graphene modified with n-hexylamine (GHA), and graphene modified with n-dodecylamine (GDA) were characterized and evaluated for their performance in removing oil component models.

Oil and organic pollutants were used as models to determine the absorption capacity of the synthesized materials. The functionalized graphene materials have efficiently absorbed oils. The separation efficiency of the oil from the water was high. The functionalized graphene, due to its branched chains, can be proven as an efficient porous material for the oil-water separation.

Introduction

Many conventional methods are being used for the separation of oil and water. The traditional methods consist of ultrasonic separation, coagulation, gravity separation, biological treatment, electrochemical treatment, skimmers, centrifugation and in situ burning[1]. The conventional methods are suffering from some serious issues of efficiencies and high cost. Oil skimmers displayed lower separation efficiencies and an expensive process. The in situ burning of oil not only destroyed the oil but also introduced secondary pollutants into the environment. Mechanical extraction is a time-consuming process and consumed a large amount of energy[2]. The inefficiency, high cost, and environmental concerns demand new methods and smart materials for efficient and eco-friendly separation of oil and water.

In oil-water separation, the super wettable materials are receiving significant attention along with a substantial increase in testing. Researchers focused their attention on improving the selective wettability of the material[2]. The super selective wettable materials that are generally used for the oil-water separation are classified as superhydrophilic and superhydrophobic materials. The superhydrophilic materials allowed the absorption or passage of water through it while oil was prevented from absorption. In the case of superhydrophobic materials, the water was prevented to pass and oil readily passed or absorbed by the material.

The surfaces are defined as hydrophilic when the water contact angle is less than 90° and hydrophobic when greater than 90°. The materials are defined as superhydrophobic if they displayed the water contact angle greater than 150°. The superhydrophobic materials are considered one of the decent opportunities for the separation of the oil and nonpolar organic contaminants from water.

The surfaces of the various support porous architecture are being modified and functionalized to achieve the surface hydrophobicity. The support materials are not limited to cotton, fabrics, meshes, and sponges/foams. The superhydrophobic surfaces were introduced by using several methodologies, including a layer by layer assembling, immersion, drop coating, hydrothermal, and polymerization. The numerous materials are utilized to improve the hydrophobicity such as graphene[3], carbon nanotubes[4], carbon nanofibers[5], metal nanoparticles, nanodiamonds, polymers, and others[6-8]. The efforts are being continued to develop cost-effective and robust materials for the efficient separation of the oil and other organic toxins from the water.

In this work, we have prepared graphene from graphite and then the obtained graphene nanosheets were functionalized with linear alkylamines. The prepared materials, graphene modified with n-propylamine (GPA), graphene modified with n-hexylamine (GHA), and graphene modified with n-dodecylamine (GDA), were characterized and evaluated for the removal of oil and organic pollutants from water.

Experimental Section

Materials

The natural graphite powder (99.9%) was commercially purchased from Fluka AG, Chemische Fabrik, Buchs (Switzerland). The sulfuric acid (H_2SO_4) (98%), hydrochloric (HCl) acid (35%), sodium nitrate ($NaNO_3$) (98%), hydrogen peroxide (H_2O_2) (30%), hydrazine hydrate (80%), and potassium permanganate ($KMnO_4$) (99%) were obtained from Sigma-Aldrich Co. (USA) and were used without further purification. The n-propylamine (PA), n-hexylamine (HA), and n-dodecylamine (DA) were purchased from Merck Schuchardt OHG (Germany) and were used as received. The cyclohexane, n-hexane, n-decane, n-heptane, and absolute ethanol (99.8%) were supplied by Sigma-Aldrich Co. (USA) and used as received. Deionized (DI) water was used throughout the research.

Synthesis of Graphene Oxide (GO)

The graphene oxide (GO) nanosheets were prepared by a modified Hummer's method. Succinctly, graphite powder (2 g) and $NaNO_3$ (2 g) were added to 90 mL of concentrated H_2SO_4 (98%) in an ice bath (0 °C to 5 °C) with continuous stirring. After 4 hours of stirring the mixture at this temperature, $KMnO_4$ (12 g) was slowly added to the suspension with care, keeping the temperature below 15 °C.

Afterward, 184 mL of DI water was slowly added to dilute the mixture and stirred continuously for 2 hours. The mixture was then stirred at 35 °C for 2 hours after removing the ice bath. The mixture was then refluxed at 98 °C for 10 to 15 minutes. After 10 minutes, the temperature was changed to 30 °C, which changed the solution color to brown. The solution was finally treated with 40 mL H_2O_2 by which the color changed to bright yellow. Following this, 200 mL of water was added and stirred for 1 hour.

It was then kept without stirring for 3 to 4 hours, where the particles settled at the bottom and the remaining water was poured to filter. The resulting mixture was washed repeatedly by centrifugation (7,000 rpm for 15 minutes) with 10% HCl acid and then followed by DI water several times until it formed a gel-like substance with neutral pH, and the supernatant was decanted away. After centrifugation, the gel-like substance was dried in a vacuum at 60 °C for at least 6 hours to obtain GO powder.

Synthesis of Amine Functionalized GO

The synthesized GO powder was dispersed in DI water (0.5 g GO/100 mL DI water), and the resulting suspension was sonicated for 1 hour prior to subsequent surface modification. Alkyl amine (about 12 g) was dissolved in 200 mL of ethanol, and then the GO water suspension was added to the alkylamine ethanol solution. The mixture was stirred continuously for a day at room temperature. The alkyl amine modified graphene was separated by centrifuge.

The reduction of alkyl amine functionalized GO was done by adding 5 mL of hydrazine hydrate, and the mixture was refluxed for 3 hours at 95 °C. The final product was washed by filtration with an ethanol-water mixture (1:1) to eliminate unreacted hydrazine hydrate or excess alkyl amine. The material was dried under vacuum at 60 °C for at least a day. The resulting solid was vacuum dried at 60 °C for at least 24 hours. A synthesis procedure was used to obtain graphene modified with GPA, GHA, and GDA materials, Figs. 1a and 1b.

Characterizations

The Fourier transform infrared (FTIR) spectroscopy of the materials were obtained using a Thermo Nicolet 6700 FT-IR spectrophotometer. Potassium bromide was ground with the sample to prepare the pellet for better resolution of the peaks. All samples were scanned in the wave number range of 400 cm^{-1} to 4,000 cm^{-1}. The Raman spectra were obtained using a Jobin Yvon Horiba LabRAM spectrometer with backscattered confocal configuration.

A long working distance objective with a magnification of 50x was used both to collect the scattered light and to focus the laser beam on the sample surface. Samples were scanned from Raman shift of 700 cm^{-1} to 2,000 cm^{-1}. The contact angles of the various hydrophobic materials were measured using an Attension Theta Flex from Biolin Scientific.

Oil Absorption Test

The weight measurements before and after oil absorption were used to evaluate the absorption capacity of the prepared materials for oil and different kinds of organic solvents. The original weight of the sample was weighed and recorded as M_i. Then, the sample was placed into various oils and organic solvents for absorption. The sample was weighed when, with the increase of absorption time, its weight was unchanged; this weight was recorded as M_t. The absorption capacity of materials, Q, for oil and various organic solvents, was calculated according to the following equation $Q(g/g) = \frac{M_t - M_i}{M_i}$.

Fig. 1a *The procedure of producing GDA.*

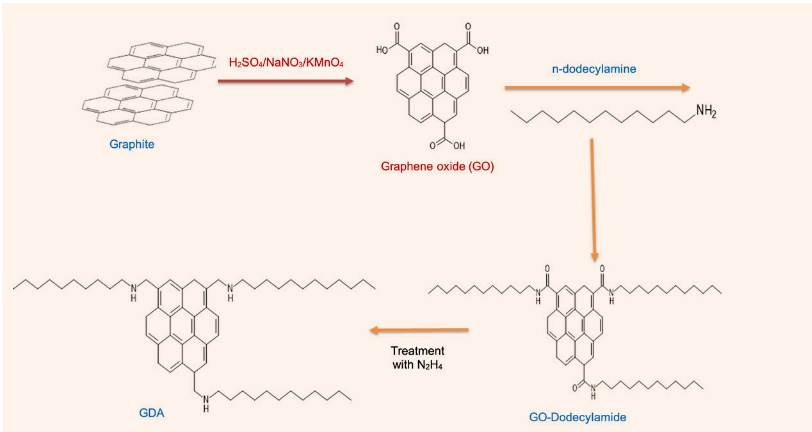

Fig. 1b *The procedure of producing GHA (left) and GPA (right).*

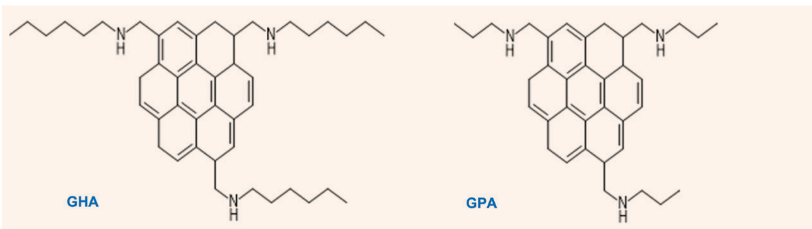

Where M_t is the weight of the material after absorption of oil or organic solvents in time, t, and the M_i of the dry material. The separation efficiency of materials was also assessed by measuring the weight percentage of the collected oil or solvent in oil-water or an organic solvent water mixture. Methylene blue dye was used to color the water layer to make it distinct from the organic layer.

Results and Discussion

Characterization

Figure 2 displays the FTIR spectrum of pure GO, which indicates the existence of some oxygen functionalities. The broad absorption peak at 3,426 cm^{-1} is attributed to the O−H stretching vibrations, which confirms the presence of the hydroxyl groups on the surface of GO and a small amount of adsorbed water molecules.

This corroborates the fact that GO is a greatly absorptive material, as proven by its tendency to become a gel-like solution. The peak at 1,724 cm^{-1} is attributed to the C=O stretching vibrations in the carboxylic groups at the edges of the basal graphene GO planes. The GO also displays two intense absorption bands at 1,225 cm^{-1} and 1,054 cm^{-1} that are respectively attributed to the C−O (alcohol) and C−O (epoxide) stretching vibrations. The peak at 1,626 cm^{-1} corresponds to the C=C bond, which shows the retention of sp^2 hybridized carbon even after the oxidation of the graphite.

Figure 2 also shows the spectra of the reduced GO functionalized with two different alkylamines as indicated. The striking difference in these spectra relative to that of GO is the disappearance of the bands corresponding to some oxygen containing functionalities. This may be attributed to the reaction of amine terminated organic molecules (R-NH_2) forming covalent linkage with the functional moieties, e.g., COOH, at the edges of the graphene sheets through amide bonding. Also, the loss of the oxygen functional peaks is indicative of the subsequent reduction of the modified GO by hydrazine hydrate.

This chemical reduction further exposes more aromatic islands at the basal plane indicated by the C=C bonds at the basal plane, which can be confirmed from the C=C stretching at ~1,630 cm^{-1}. In addition, the band at 3,426 cm^{-1} in GO shifts somewhat to 3,435 cm^{-1} with symmetric peak shape and less intense peak, which may be indicative of the N–H stretching of the grafted amine onto GO via the amidation reaction. The doublets at 2,921 cm^{-1} and 2,853 cm^{-1} correspond to the asymmetric and symmetric C–H vibrations of the alkyl groups, respectively.

Raman spectroscopy gives an overview of the morphology of carbon-based materials. There are two prominent bands for such materials, such as the D and G bands, Fig. 3. The G model, which is peaked at 1,587 cm^{-1} corresponds to the in-plane vibrations of the sp^2 hybridized carbon atoms present in both rings and chains. The disorder band (D band) at 1,331 cm^{-1} is indicative of the structural disorder caused by the sp^3 carbon atoms covalently bonded to the epoxide and hydroxyl functionalities in the GO basal plane.

The ratio of the peak intensity of the D to G bands, I_D/I_G, is used to evaluate the extent of disorder in the graphene-based material. The higher D band indicates the breaking of the sp^2 bonds and forming of the new sp^3 bonds. Figure 3 also displays the Raman spectra of the GO and amine functionalized GO. The I_D/I_G, for GDA (I_D/I_G = 1.41), GHA (I_D/I_G = 1.40) and GPA (I_D/I_G = 1.31), increased compared to that for GO (I_D/I_G

Fig. 2 *The FTIR spectra of the prepared materials.*

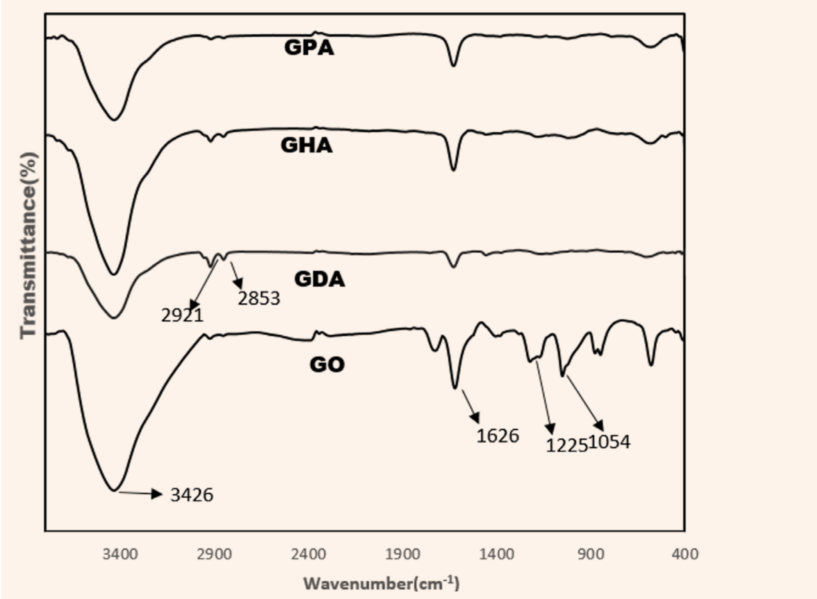

Fig. 3 *The Raman spectra of the prepared materials recorded using 633 nm laser excitation.*

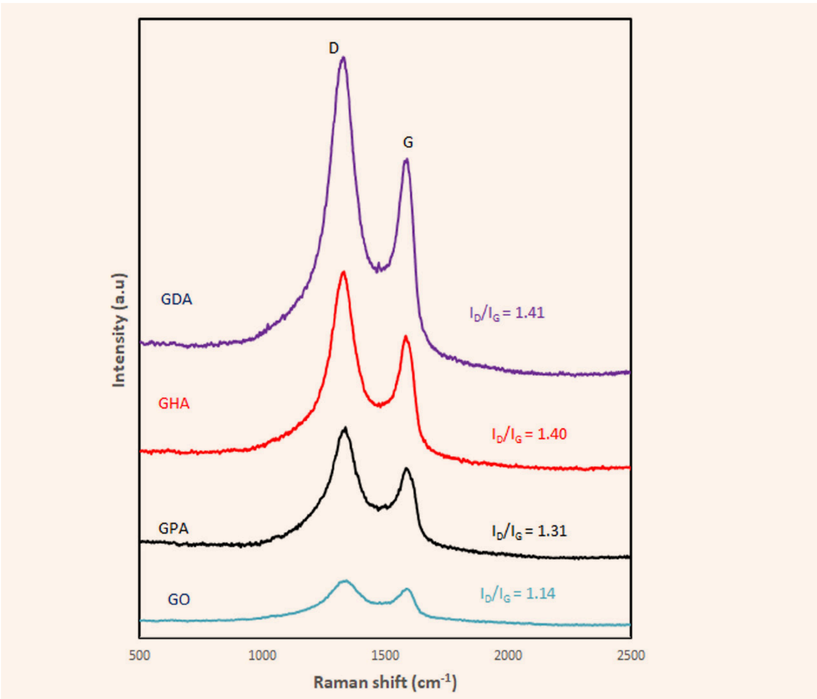

= 1.14). This fractional increase in peak intensity ratio demonstrates that new defects are produced during the functionalization of the GO.

Absorption Performance of the Material

Experiments were carried out to assess quantitatively the oil absorption performance of the three amine functionalized graphene materials. In typical absorption capacity measurements, oil and common organic pollutants, including decane, cyclohexane, and hexane, were selected as pollutant models. In this test, the materials were placed in a beaker containing oil or organic solvents to be absorbed. Each material was submerged under 10 mL of the absorbate and pressed in the liquid for maximum oil absorption. The materials were then taken out and compressed manually with the aid of a quick-grip clamp.

The absorption capacity is greatly dependent on the porosity of the materials. More porous structures will afford high liquid absorption. Therefore, materials with higher hydrophobicity will absorb organic liquids more readily and separate oil from water more effectively. Figure 4 presents the absorption capacities of the amine functionalized materials for the oil and the nonpolar solvents, which are 25 to 65 times its own weight, based on the density and viscosity of the oil and solvents. The oil absorption performance and high selectivity are associated with the porous structures and the superoleophilic and superhydrophobic nature of the GDA oil absorption films, which show four to 16 times higher than GHA and GPA films, most especially for cyclohexane.

GPA had the lowest absorption capacities in all the tests; this could possibly be due to the increase of hydrophilicity — based on the existence of more nitrogen molecules in n-dodecylamineohexane — of the composite material. The GDA displays excellent absorption capacities ranging from 34 to 64 times its own weight for all the absorbates used. Significantly, the GDA showed greater absorption capacity than many sorbents in previous reports, such as polymers (5-25)[9], polydimethylsiloxane sponge (four to 11 times)[10], reduced GO foams (five to 40 times)[11], and chitin sponge (30 to 60 times)[12]. The absorption capacity in other materials is higher than that of the GDA, such as graphene modified foam (60 to 140 times), cellulose nanofiber aerogel (106 to 312 times)[13], and ultra-flyweight aerogel (215 to 913 times)[14].

The simple, low-cost and easily large-scale fabrication method make GDA an excellent candidate to be used as an absorbent for oil spill cleanup and organic pollutants.

Oil-Water Separation

The oil-water separation test of the prepared materials was performed by dipping the material in the oil or solvent/water mixture (5 mL, 45 mL). As the materials approached the mixture, it selectively and quickly absorbed the floating solvent or oil on the surface of the water, leaving behind water in the system. The material tended to float on the surface despite being immersed by an external force to achieve higher separation efficiency, Fig. 5.

The graphene modified materials instantly absorbed the organic phase once the material was in contact with the oil or the solvent. The differential affinity to the organic layer (oil or solvent phase) clearly showed that the materials had oleophilic and hydrophobic characteristics, where the organic solvent or oil could flow into the material pores easily and rapidly. This clearly showed the superhydrophobic nature of the GDA.

The oil could be recovered by a simple mechanical squeezing method and the materials could be reused repeatedly. The efficiency of separation of the hydrophobic and oleophilic GDA for the organic solvents and oil is high.

Fig. 4 *The absorption capacity (weight gain) of all the modified graphene materials in the oil and in the organic liquid media.*

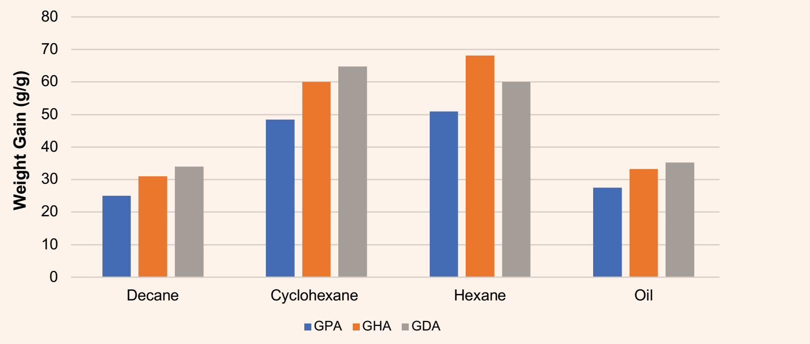

Fig. 5 *The separation efficiency of the modified materials for different types of the oil-water mixture.*

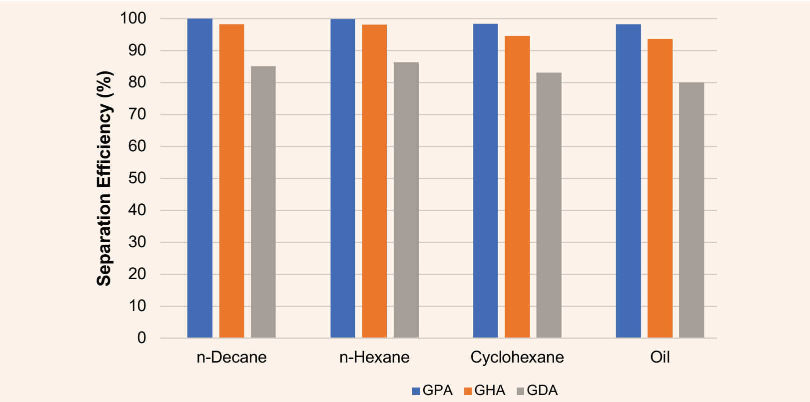

Further Evaluation of the GHA and GDA Material

To evaluate and measure the absorbability of the GHA and GDA material, experiments were conducted several times with three different hydrocarbons — hexane, heptane, and octane — on the same material sample.

The procedure that was used is as follows:

1. The initial weight of the material was measured.
2. The material was then dipped in a mixture 20:2 of dyed water and hydrocarbon for several minutes until the hydrocarbons were fully adsorbed.

Table 1 *The absorption capability with hexane, heptane, and octane.*

Experiment	Hydrocarbon	Time of Full Adsorption	Initial Weight of Material	Wet Material Weight	Specific Gravity (g/mL)	Actual Adsorbed Hydrocarbon in mL	Comments
1	2 mL hexane	5 min	0.28	1.3 g	0.659	2 mL	Complete adsorption of hydrocarbon
2	2 mL heptane	5 min	0.28	1.2 g	0.6838	1.75 mL	Complete adsorption of hydrocarbon
3	2 mL octane	10 min	0.28	1.14 g	0.692	1.64 mL	Slightly less hydrocarbon adsorbed

3. The final weight of the material and time of adsorption was noted.
4. Then the material goes through the desorption process from the hydrocarbon.
5. The material initial weight should be measured again to make sure that there are no hydrocarbons left.
6. Repeat from step 2 with a different hydrocarbon.

The material showed that high hydrocarbon absorptivity and a 100% water rejection can adsorb up to three times its initial weight of hydrocarbons from water within a short time. The material can then be easily recycled for reuse.

Table 1 lists the test results for the absorption capability with hexane, heptane, and octane.

Conclusions

In this article, three stable and robust types of graphene, modified with linear alkylamines, including n-propylamine, n-hexylamine, and n-dodecylamine, were characterized and their performance evaluated by absorption and oil water separation tests.

The absorption capacity is greatly dependent on the porosity of the materials. Therefore, the material with higher hydrophobicity will absorb organic liquid more readily and will have higher oil/water separation efficiency.

- GDA oil absorption is four to 10 times higher than GHA and GPA, due to its higher porous structure and its superoleophilic and superhydrophobic nature.
- The GDA displays excellent absorption capacities ranging from 34 to 64 times its own weight for all the absorbates used.
- The GPA showed the lowest absorption capacity in all tests.
- An oil-water separation test was conducted on the three graphene modified materials, whereby the organic pollutant (oil) in the water was instantly absorbed.
- Oil can be recovered from the materials by using the mechanical squeezing method while the material can be reused for oil from water absorption.
- The efficiency of separation of the hydrophobic and oleophilic GDA for the organic solvents and oil is high — up to 99.9% — while in the GHA and GPA, it is up to 98% and 83%, respectively, depending on the organic pollutant.

Acknowledgments

The authors would like to thank Prof. Tawfik A. Saleh from the Chemistry Department at King Fahd University of Petroleum and Minerals, for his work toward this article and his collaboration for supporting several material syntheses projects to enhance oil-water separation.

References

1. Lei, Z., Deng, Y. and Wang, C.: "Multiphase Surface Growth of Hydrophobic ZIF-8 on Melamine Sponge for Excellent Oil/Water Separation and Effective Catalysis in a Knoevenagel Reaction," *Journal of Materials Chemistry A*, Vol. 6, Issue 7, January 2018, pp. 3258-3263.
2. Qiu, S., Hou, L., Liu, J., Guo. F., et al.: "High-Flux, Continuous Oil Spill Collection by Using a Hydrophobic/Oleophilic Nanofibrous Container," *RSC Advances*, Vol. 7, Issue 32, April 2017, pp. 19434-19438.
3. Zhang, L., Li, H., Lai, X., Su, X., et al.: "Thiolated Graphene-Based Superhydrophobic Sponges for Oil-Water Separation," *Chemical Engineering Journal*, Vol. 316, May 2017, pp. 736-743.
4. Gu, J., Xiao, P., Huang, Y., Zhang, J., et al.: "Controlled Functionalization of Carbon Nanotubes as Superhydrophobic Material for Adjustable Oil/Water Separation," *Journal of Materials Chemistry A*, Vol. 3, Issue 8, 2015, pp. 4124-4128.
5. Baig, N., Alghunaimi, F.I. and Saleh, T.A.: "Hydrophobic and Oleophilic Carbon Nanofiber Impregnated Styrofoam for Oil and Water Separation: A Green Technology," *Chemical Engineering Journal*, Vol. 360, March 2019, pp. 1613-1622.
6. Li, J-J., Zhou, Y-N., Jiang, Z-D. and Luo, Z-H.: "Electrospun Fibrous Mat with pH-Switchable Superwettability that can Separate Layered Oil/Water Mixtures," *Langmuir*, Vol. 32, Issue 50, November 2016, pp. 13358-13366.
7. Baig, N., Alghunaimi, F.I., Dossary, H.S. and Saleh, T.A.: "Superhydrophobic and Superoleophilic Carbon Nanofiber Grafted Polyurethane for Oil-Water Separation," *Process Safety and Environmental Protection*, Vol. 123, March 2019, pp. 327-334.

8. Lin, B., Chen, J., Li, Z-T., He, F-A., et al.: "Superhydrophobic Modification of Polyurethane Sponge for the Oil-Water Separation," *Surface and Coatings Technology*, Vol. 359, 2019, pp. 216-226.

9. Carreira, L.G., Mendes, L.C., Ribeiro, M.R.G. and Sebastião, P.J.: "Organically Expanded Graphite/Octadecylamine: Structural, Thermal and Relaxation Evaluation," *Materials Sciences and Application*, Vol. 4, Issue 5, May 2013, pp. 281-286.

10. Sonmez, H.B. and Wudl, F.: "Cross-Linked Poly(orthocarbonate)s as Organic Solvent Sorbents," *Macromolecules*, Vol. 38, Issue 5, February 2005, pp. 1623-1626.

11. Choi, S-J., Kwon, T-H., Im, H., Moon, D-I., et al.: "A Polydimethylsiloxane (PDMS) Sponge for the Selective Absorption of Oil from Water," *ACS Applied Materials and Interfaces*, Vol. 3, Issue 12, November 2011, pp. 4552-4556.

12. Niu, Z., Chen, J., Hng, H.H., Ma, J., et al.: "A Leavening Strategy to Prepare Reduced Graphene Oxide Foams," *Advanced Materials*, Vol. 24, Issue 30, August 2012, pp. 4144-4150.

13. Duan, B., Gao, H., He, M. and Zhang, L.: "Hydrophobic Modification on Surface of Chitin Sponges for Highly Effective Separation of Oil," *ACS Applied Materials and Interfaces*, Vol. 6, Issue 22, October 2014, pp. 19933-19942.

14. Wu, Z-Y., Li, C., Liang, H-W., Chen, J-F., et al.: "Ultralight, Flexible, and Fire-Resistant Carbon Nanofiber Aerogels from Bacterial Cellulose," *Angewandte Chemie International Edition*, Vol. 52, Issue 10, March 2013, pp. 2925-2929.

About the Authors

Norah W. Aljuryyed

B.S. in Chemical Engineering, Teesside University

Norah W. Aljuryyed joined the Production Technology Division in Saudi Aramco's Exploration and Petroleum Engineering Center – Advanced Research Center (EXPEC ARC) in December 2018. Her focus is on water conservation and stimulation technology to enhance acidizing and fracturing fluids' recipe.

Norah works on several research projects striving to utilize different water sources and develop economical water treatment methods for upstream applications.

In 2018, she received her B.S. degree in Chemical Engineering from Teesside University, Middlesbrough, U.K. Norah also holds a diploma in Technical Chemistry form Vienna University of Technology, Vienna, Austria. Her under graduate research focused on designing a hydrogen production plant with a small modular reactor.

Dr. Fahd I. Alghunaimi

Ph.D. in Chemical Engineering, King Abdullah University of Science and Technology

Dr. Fahd I. Alghunaimi is currently the Productivity Enhancement Focus Area Champion with the Production Technology Division of Saudi Aramco's Exploration and Petroleum Engineering Center – Advanced Research Center (EXPEC ARC). His area of expertise is crude oil separation and water treatment.

Fahd's recent work in oil removal from produced water was selected by the Institution of Chemical Engineers (IChemE) as a finalist in the Oil and Gas Category of the 2021 Global Energy Show Awards. Also, his work in water treatment was highly commended for the 2020 IChemE Water Global Award.

Fahd has published more than 30 technical papers, disclosed more than 15 patents, deployed several technologies, received eight international awards, presented several conference papers, and has more than 650 citations.

He received his Ph.D. degree in Chemical Engineering from the King Abdullah University of Science and Technology, Thuwal, Saudi Arabia.

Improved Sand Fill Cleanout Utilizing an Integrated Vacuuming System and Real-Time Monitoring in Horizontal Extended Reach Wells

Hussain A. Almajid, Alaa S. Shawly and Usman Ahmed

Abstract /

A variety of clean out methods have been developed in the past to remove scale and sand fill accumulation from the wellbore section to restore the well's potential. The success rate for such an operation is impacted by multiple factors, such as fluid properties, limited annular velocities, particle size, reservoir pressure, and wellbore diameter. In addition, this process commonly involves applying excess hydrostatic pressure on the formation to circulate wellbore fluids, which can result in lost circulation and formation damage.

This article will share the technical details along with the field results for a novel vacuuming system with integrated real-time data, which can be operated in three different modes, to remove both undesirable liquids and solids. The process involves pumping a low-cost clean out fluid down the internal string through a jet pump and venturi nozzle assembly. A localized pressure drawdown is created at the bottom-hole assembly (BHA), drawing wellbore liquids and solids into the return flow, and the entrained flow is returned up the outer coiled tubing (CT) string to the surface.

Several clean out jobs have been successfully performed in the field using this technique. The use of empirical correlations have been developed and incorporated into an existing proprietary solids transport computer algorithm, which played a vital role in the optimization of the hole cleaning process. Post-job results will be discussed in this article, including the fill diagnostic process, an assessment of the clean out method, the job design, selection of fluids, CT BHA tools, job execution, field experience, and post-clean out performance evaluation.

This article will describe a reliable alternative combining an integrated vacuuming system and real-time monitoring that can effectively remove scale and sand fill accumulation caused by excessive sand production and fines migration in a large wellbore diameter, where annular fluid velocity and lifting efficiency is a major challenge.

The novelty of this approach is its ability to create a wellbore vacuuming system that can provide efficient lifting capabilities while eliminating the need for high cost fluids and large quantities of nitrogen in deep horizontal extended reach wells. Recommendations and lessons learned from several field cases are also shared to further improve the clean out process.

Introduction

Sand production is a common problem faced by many oil and gas producers and water injectors worldwide. Sand migration into the wellbore often results in a reduction of production or injection rates. Several clean out methods have been developed over the decades employing a number of different techniques, incorporating high circulation rates, special circulating fluids, wiper trips or reverse circulation to remove solids from the wellbore and up to the surface.

Many of these conventional sand clean out methods often require the use of high circulation rates, which applies excessive downhole pressure on the formation and could result in lost circulation return, especially in pressure depleted reservoirs. The conventional solution to overcome depleted hydrostatic pressure has been to include nitrogen to reduce fluid density, and thereby decrease the hydrostatic head; however, this necessitates a very specific job design and execution and can require large amounts of liquid nitrogen in the case of horizontal wells, possibly jeopardizing the success rate of such operations.

Vacuuming Process Mechanism

The evolution of wellbore vacuuming technology has brought a unique solution to this problem. The sand/well vacuuming technology has been developed and proven by field operations worldwide to clean out wellbores with a low bottom-hole pressure (BHP). The sand/well vacuuming system consists of a specialized downhole jet pump connected to a concentric coil tubing (CCT) string, Fig. 1. The clean out fluid is circulated down the central string and returned via the CCT annulus[1, 2].

Fig. 1 *A process illustration for the CCT with a specialized jet pump.*

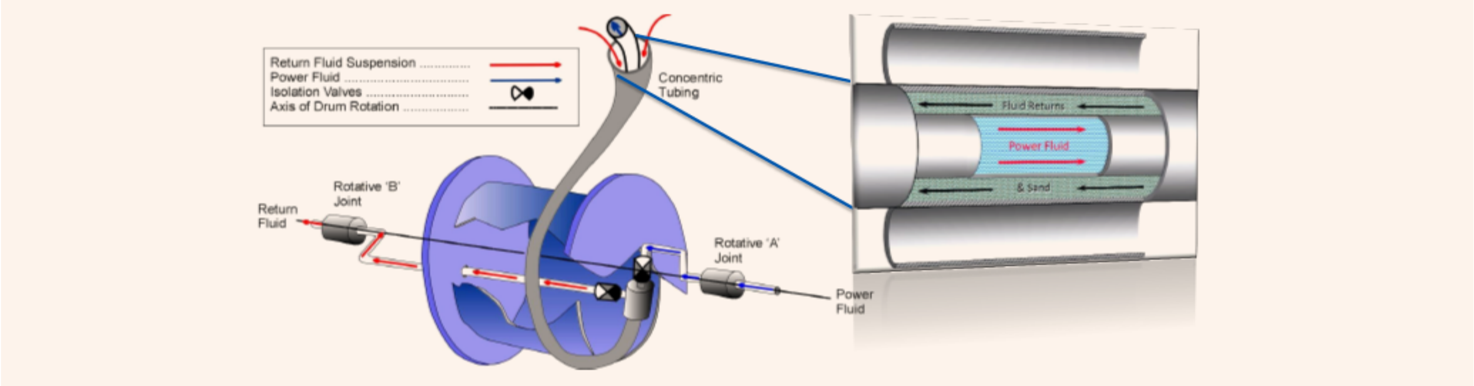

The action of power fluid passing through the jet pump and venture assembly essentially vacuums the formation liquid and fill out of the wellbore, and this combined flow of sand/fluid returns up the CCT annulus without placing any additional hydrostatic pressure on the formation. The advantage of this system is that the velocities of the return fluid are relatively high due to the small annular areas involved, therefore, the sand/return fluid is not allowed to settle out while circulation is maintained.

The main components of a jet pump are the power nozzle, throat, and diffuser, Fig. 2. High-pressure fluid at a low velocity passes through a nozzle into a throat, where the change into a high velocity and low-pressure creates a Venturi effect[3, 4]. This jet pump has been optimized to accommodate variation in both intake rates and drive pressures, based on the fluid rates attainable through the internal CT string, thereby creating a system that does not rely on the formation hydrostatic pressure during the sand/wellbore vacuuming process.

Although the jet pump can be driven with a variety of different liquids, a mixture of formation water with oil dispersant and friction reducer is best suited for optimum lifting applications. Also, there is no need to circulate nitrogen to reduce the hydrostatic pressure since there is no hydrostatic pressure acting on the formation during the sand/well vacuuming clean out process.

This tool is operated in three modes, which are sand removal, fluid recovery, and forward jetting mode. In the sand removal mode, a portion of the pumped fluid is diverted through the external, front, and rear facing swirl jets to fluidize the sand for easier removal, Fig. 3. During the fluid recovery mode, or well vacuuming mode, the external swirl jets are shut off, resulting in an increased pressure drop across the nozzle throat and greater wellbore fluid being unloaded from the well.

While in the forward jetting mode, the pumped fluid flows through the forward nozzles, creating a higher jetting velocity to break consolidated sand bridges or to displace treatment fluids into the wellbore, Fig. 4. Consequently, the tool can be alternated between these modes by pressure cycling as many times as necessary until all fill has been recovered from the wellbore. Typically, the tool would be run in the hole (RIH) using the sand removal mode initially while entering into the fill accumulation and then the clean out process is switched to the fluid recovery mode at the toe of the well while pulling back through the horizontal section.

This sand/well vacuuming system provides a localized pressure drawdown at every point in the wellbore that the tool passes, which allows for an effective sand removal in the sand vacuuming mode as well as removing any accumulated mud filter cake deposits in the well vacuuming mode. Memory gauges can be run as part of the bottom-hole assembly (BHA) to record downhole parameters, such as pressure and temperature. This data can be used to perform pressure buildup analysis and evaluate the productivity index along the entire horizontal treated section, thereby allowing us to identify zones with severe formation damage, and consequently, the operator may choose to perform on-site treatment stimulation and optimization.

Although the cleanup treatment with the CCT does not prevent the sand deposition in horizontal wells, it does considerably prolong the period between recurrent

Fig. 2 *The main components for the CCT downhole jet pump.*

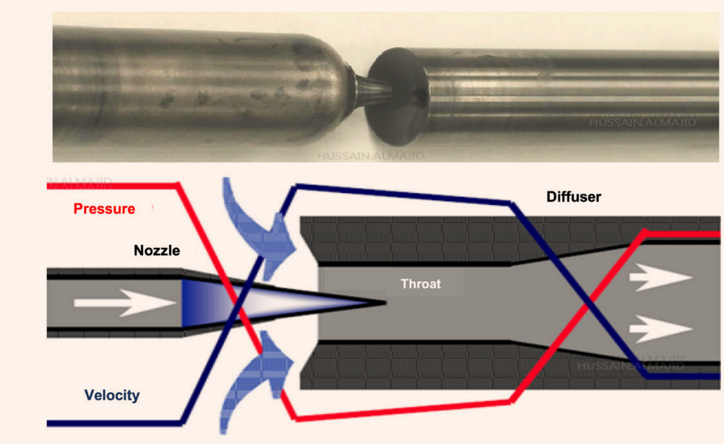

Fig. 3 *A demonstration of the tool operation in the sand vacuuming mode.*

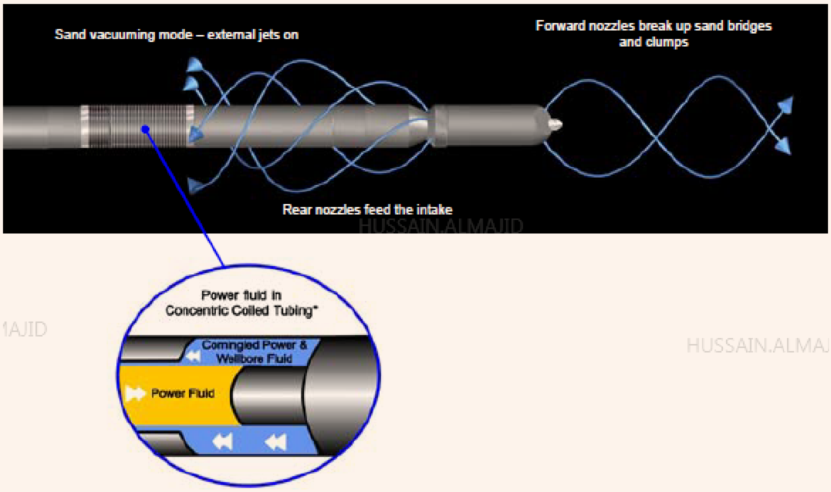

Fig. 4 *A demonstration of the tool operation in forward jetting mode.*

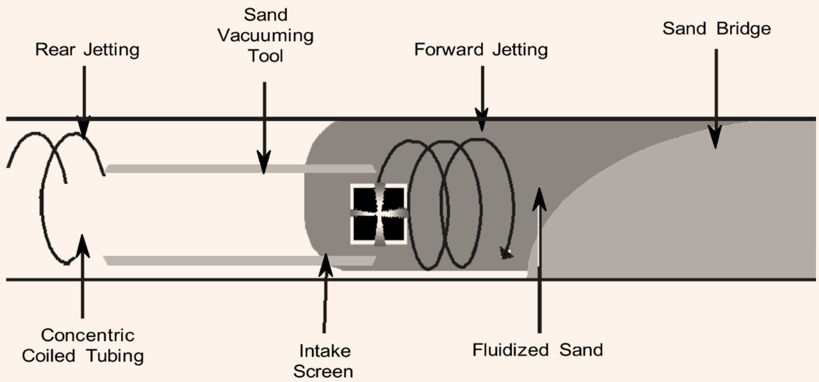

workover necessities. The average time before reoccurrence of workover activity due to the sand production in horizontal wells after they have been treated immediately after drilling is about two times greater than for the wells that have not been treated[5, 6]. There is a longer life expectancy of the lifting equipment and tubulars in cleaned up wells.

Well Completion Details

Well-A was drilled in an unconsolidated sandstone formation with heterogeneous rock properties. The well was developed as a water injector to enhance sweep efficiency and oil recovery. The well was completed with 9⅝” casing extending from the surface up to an intermediate depth point and 7” casing from 9⅝” end up to the top of the injection interval. Meanwhile, the lower completion consisted of a 4½” perforated liner across the entire injection interval up to the plug back total depth (PBTD). Consequently, sand accumulation/influx from the reservoir would occasionally occur when the well was shut-in. As a result, the well performance will be impacted, as observed in the drop-in injection rate and increase in injection pressure.

Sand/Well Vacuum Simulation Model

A detailed planning and review process was implemented prior to commencing clean out operations in the selected wells completed with large diameter casings. A computer software simulator has been developed to integrate the correlations for sand concentration and hole cleaning time in the annulus of the CCT string. A computational approach using calculated volumes was adopted and empirical formulas were applied to predict the pressure, fluid velocities, and solids transport efficiency. Fluid properties and flow rates are used to predict the solids removal rate, which is then integrated in time to give the solids concentration of each control volume[7, 8].

The simulator allows the user to predict the time history of in situ solids concentrations along the CCT annulus and the hole cleaning time for a given operational case.

This is an essential tool for field engineers to successfully design and execute the sand/well vacuuming operations. The model allows for on-site real-time monitoring of downhole pressure and temperature readings. The model also provides the overall sand/well vacuuming fluid dynamics and aids in optimizing and predicting the mechanical performance envelope, operating rates, pressures, velocities, sand pickup rates, and CCT stress conditions.

The pull out of hole (POOH) speed, backward jetting velocity, and distance between the tool intake and backward nozzles are all key parameters to ensure high clean out efficiency. Once the maximum distance between the tool intake and backward nozzles is exceeded, the pumping fluid will not be able to fluidize the sand bridges and receive them at the intake due to the longer distance it takes for the sand to travel before it reaches the intake. Conversely, if the distance between the tool intake and backward nozzles was too small, then the sand particles will bypass the tool intake screen and they will be left behind in the wellbore. Consequently, maintaining the required speed while POOH is key to ensure an efficient hole cleaning process by allowing ample time for wellbore clean out at each stage.

Once sand particles enter the sand vacuuming BHA, the particles are transported to the surface through the annulus of the CCT string. Comprehensive simulations must be performed to accommodate for the velocity, deviation angle, particle size, density, fluid density, and viscosity, thereby ensuring that these solids are transported all the way to the surface.

Job Design and CCT Size Selection

A key element in the CCT size selection process is to maximize penetration and reach depth into the wellbore, due to the large wellbore diameter casing/open hole section for these extended reach horizontal wells. The selected CCT was a 0.095" wall thickness, 1" inner string by 0.156" wall thickness, and a 2" outer string with a total length of X682 ft. This large outer CCT size allows for additional lateral coverage and higher circulation flow rates while increased boost pressure are achievable down the smaller size inner string, thereby ensuring that all returning fluids and solids are not lost along the long annular flow path.

The fluid system utilized for the clean out was a water mixed with a concentrated friction reducer fluid for extended CCT reach. The selected power fluid had an excellent shear thinning property that exhibited low viscosity when pumped through the CCT and high viscosity with strong carrying capabilities when it is subjected to a low shear rate. The power fluid pumping rate through the 1" inner string averaged 0.4 bbl/min at 5,000 psi injection pressure.

The jet pump nozzle and throat size were optimized to create adequate intake suction while providing stable return pressures up the CCT annulus. It was designed to avoid losing the fluids into the formation and was achieved on location by monitoring fluid pumped vs. fluid return volumes during sand recovery operations. If a 1:1 ratio was not maintained, the vacuum tool would be switched from sand vacuum mode to well vacuum mode to recover the fluid lost to the wellbore.

Due to the low pumping rates in the system, the solids inflow into the vacuum tool must be controlled to ensure continuous surface returns. Typical RIH speeds for the operation were between 1 ft/min to 2 ft/min, maintaining solids intake of 1% to 2% by mass. Fluid velocities in the concentric annulus were approximately > 50 in/sec, which exceeds the minimum for solids transport.

Table 1 lists the CCT size selection with the corresponding pumping and suction rates.

Table 1 *CCT size selection with the corresponding pumping and suction rates.*

CCT Size (in)	Pump Pressure (psi)	Wellhead Pressure (psi)	Switch Orifice Size (in)	Bypass Orifice to Swirl Nozzles (in)	Main Nozzle Size (#)	Throat Size (#)	Suction Rate (L/min – bpm)	Main Nozzle (L/min – bpm)	Swirl Nozzles (L/min – bpm)
1 × 2	3,000	20	0.221	0.08	4	3	20.00 – 0.13	33.03 – 0.21	19.81 – 0.12
1 × 2	3,000	20	0.221	0.08	5	4	20.00 – 0.13	37.49 – 0.24	18.51 – 0.12
1 × 2	3,000	20	0.221	0.08	6	6	24.00 – 0.15	40.02 – 0.25	17.72 – 0.11
1 × 2	3,000	600	0.221	0.08	4	2	18.00 – 0.11	37.94 – 0.24	15.11 – 0.10
1 × 2	3,000	600	0.221	0.08	4	3	28.00 – 0.18	35.22 – 0.22	16.00 – 0.10
1 × 2	3,000	600	0.221	0.08	5	4	31.00 – 0.20	40.18 – 0.25	14.34 – 0.09
1 × 2	3,000	600	0.221	0.08	6	5	33.00 – 0.21	43.04 – 0.27	13.29 – 0.08
1 × 2	5,000	600	0.221	0.08	7	5	28.00 – 0.18	64.52 – 0.41	16.15 – 0.10
1 × 2	5,000	600	0.221	0.08	7	6	45.00 – 0.28	63.09 – 0.40	16.73 – 0.11

Operational Safety Precautions

CT fatigue is a major concern when planning conventional sand clean out operations, especially with large diameter CT strings. This issue is not a major concern for the CCT sand/well vacuum mode since the outer CT experiences minimal surface pressure created by the returned flow path. Subsequently, its fatigue life is extended beyond the normal fatigue life of a typical 2" CT work string. Conversely, the inner string is exposed to a relatively high internal pressure. Due to its smaller diameter, the 1" CT has a fatigue life that is four times that of the 2" outer string in this operation.

Well-A is drilled and completed into a formation zone with low hydrocarbon gases present. As such, additional precautions were taken to divert any produced gas from the CCT annulus to the surface testing and flare systems for gas handling, Fig. 5. Further entrainment of produced gas can be stopped at any time by shutting down the power fluid pump. This will remove the concentric annulus boost pressure, allowing fluids from the CCT to essentially kill the well. Additionally, pumped fluid could be diverted down the inner string, the CCT annulus, the CCT by production tubing annulus, or any combination to quickly displace any produced gas. To further mitigate this situation, a combination shear/blind ram was incorporated in the well control stack as a last resort.

Several formal risk assessments were completed regarding personnel and equipment safety as well as environmental controls. Some items of note are:

- Temporary wind walls installed around the platform deck to decrease liquid splatter by wind gusts.
- Fluid containment pads surrounded the wellhead and CT equipment.
- A containment system was installed around the CT injector to prevent any lubricant or other fluids from reaching the Cook inlet.
- Land operations would have drip pans installed under all units.

Job Execution

Previous clean out attempts using a conventional sand removal method proved to be ineffective in Well-A due to large downhole completion design and low reservoir pressure that have made the lifting process very challenging. This well is completed with a 4½" (internal diameter (ID) is 3.958") screen liner from top of the injection interval up to PBTD and a 7" casing (ID is 6.276") from a 9" casing shoe up to the top of the injection interval. The main challenge encountered in the previous conventional clean out methods was that the annular velocity required to lift the sand all the way to the surface could not be sustained inside the large ID of the 7" casing, which deemed the clean out ineffective. The advantage of the CCT sand/well vacuum mode is that the annular space between the 2" outer string and 1" inner string is small enough to lift the sand to the surface.

During the job, the CCT BHA was alternated between the sand vacuum mode and well vacuum cleaning mode up to the maximum reach depth at PBTD. At this stage, clean out attempts were carried out by utilizing both the CCT BHA and by pumping different mixtures of

Fig. 5 The implemented surface testing layout for return monitoring and handling.

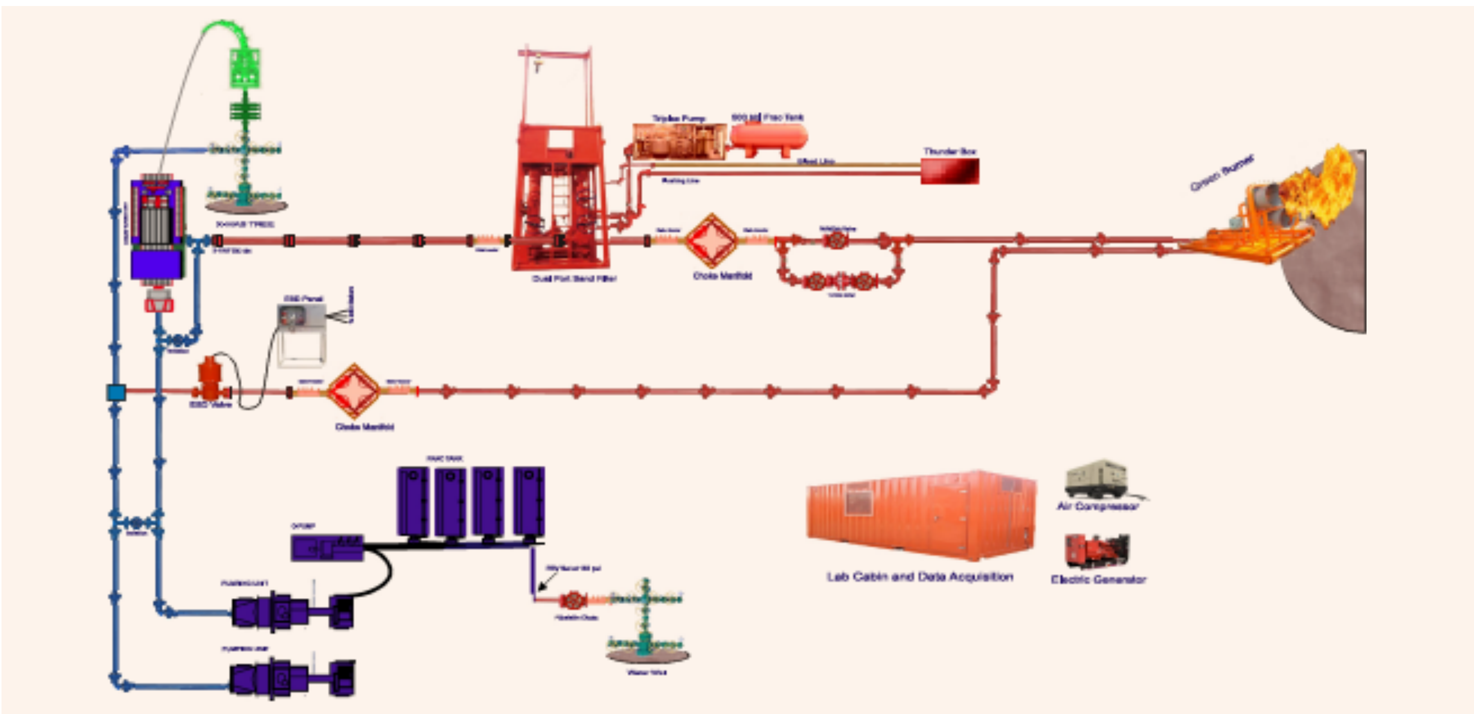

clean out fluids, such as mutual solvent fluids and 15% HCl acid. This procedure was repeated in steps and by allowing the clean out fluids to soak in the well and break the hard sand bridge prior to attempting RIH again until a maximum reach depth at PBTD, Fig. 6. Meanwhile, the testing was getting sand up to 60% by weight, which confirmed that the 7" liner was being completely cleaned. A sand filtration system was installed in the upstream on the choke manifold, but it was bypassed during the operation as it was inducing additional back pressure on to the system, which negatively impacted the lifting process. The fluid return rates were below the manufacturer's minimum limit and the small particle size of the solids made it difficult to detect.

Overall, the conducted vacuuming treatment job was effective in removing 500 ft of sand fill accumulation and improved the well productivity index with the total recovered sand column from the 7" liner while minor precipitates were detected during flow back operations. The well was put on injection following the treatment, and performance analysis showed a steady increase in injection equivalent to 50% improvement prior to treatment implementation.

Sand/Well Vacuuming Process Operational Enhancements

The feasibility and success rate of wellbore vacuuming operations on a depleted well utilizing CCT depends on multiple parameters, including the downhole tool, utilized equipment, operational planning, and field personnel experience. The following are a list of best practices to be considered for future sand/wellbore clean outs utilizing CCT:

1. A sophisticated computer simulator must be used to select the proper tool setup of CCT string size and optimize the complete sand/well vacuuming process. The software can be utilized to predict various important parameters for the operation such as injection pressure, surface flow rates, sand and fluid suction rate, external jetting rate, return rate and sand load in the CCT annulus, and inlet and outlet pressure of the jet pump, and the CCT RIH and POOH speed.
2. Monitoring the injection pressure, injection flow rate, and return rate is crucial to ensure that the downhole jet pump is working properly. If the power nozzle or throat is worn out, the jet pump loses suction rate, and therefore, the return rate would drop off considerably for a given operating condition. In some cases, downhole junk material or wellbore scale may block the intake screen causing the suction rate to drop off as well.
3. If the liquid return rate is less than the injection rate for a while in the sand vacuuming mode, it may indicate that the fluid is being lost into the well. The vacuum tool should be switched from the sand vacuuming mode to the well vacuuming mode to recover the lost fluids.
4. Wellbore conditions near the top of the fill can be verified by running the CCT in hole in using well vacuuming mode or with no circulation. Since there is no external forward jetting near the end of the BHA, the tool will prevent movement of the CCT in hole as soon as any significant amount of solids are encountered. In addition, RIH without circulation until reaching the top of the fills would prevent the nozzle/throat pre-wear out.
5. A proper mechanism for volumetric measurement of the recovered sand at the surface must be implemented

Fig. 6 *Clean out treatment stages implemented at Well-A utilizing the CCT.*

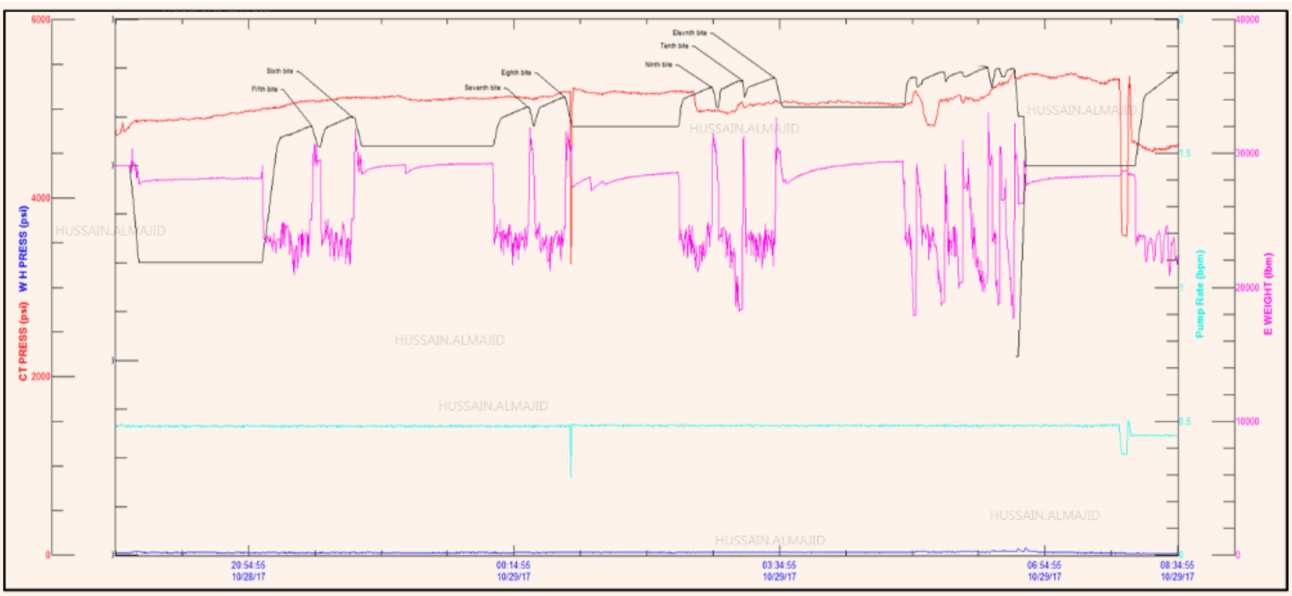

to accurately measure the return volume and determine if the circulation rates are matching with the return rate, and consequently identify if any fluid is being lost into the formation.

6. A CCT mill and motor can be run as a contingency plan in case downhole obstructions are encountered and it is required to extend the reach depth into the wellbore. Similarly, chemical dissolution alternatives may be used to dissolve hard bridge material provided that proper surface testing equipment are available to treat the return fluids.

7. Fluid sampling and downhole memory gauges are valuable tools in the evaluation of the production profile along the wellbore and as a diagnostic tool in case of potential well problems.

Conclusions

This article discusses a downhole vacuuming technology application in low reservoir pressure, large casing diameters for sand removal operations, and demonstrated how to effectively remove sand fill accumulations from challenging wellbore conditions. The engineering challenges, best practices and lessons learned from these vacuuming operations are summarized. Post-job analysis indicates that this technology is a viable and effective means to remove sand fill from wellbores with large completion and low BHP.

The following points summarize the lessons learned, cultivated from the implemented field applications.

1. The downhole vacuuming technique proved to be a successful method to efficiently remove sand fill accumulations from the low BHP wells and large diameter completion. The final assessment for the developed tool application concludes that it can be operated in low BHP scenarios with minimal pump wear.

2. The sand/well vacuuming process provides an effective solution to remove sand fill accumulation without creating any overbalance pressure on the formation that could result in fluid loss, thereby creating formation damage.

3. A modified design with a high-pressure drop, rotational jetting tool and a downhole motor with a mill can be combined in the sand vacuuming BHA to increase penetration into the formation whenever hard sand bridges are encountered.

4. Utilization of water mixed with oil dispersant and friction reducer helped to extend CCT reach depth in extended horizontal section wells.

5. This vacuuming tool can be alternated between sand vacuuming and forward jetting as many times as needed during the operations, depending on the wellbore conditions and rigidness of fill material to facilitate breaking sand bridges and to properly clean out the well.

6. Using updated software with real-time field data, and considering the parameters involved in the sand/well vacuuming process, can help field engineers to design, optimize, and execute the vacuuming process efficiently.

Acknowledgments

This article was presented at the International Petroleum Technology Conference, Riyadh, Kingdom of Saudi Arabia, February 21-23, 2022.

References

1. Thomas, C.P., Daughty, T.C., Fauler, D.D. and Hite, D.M.: "South-Central Alaska Natural Gas Study," U.S. Department of Energy Report, 2004, 207 p.

2. Ledlow, L.B. and Seitz, B.T.: "Application and Performance of Single-Trip, Multi-Zone, High Rate Water Packs in a Mature Low-Pressure, Low Temperature Gas Field," SPE paper 86512, presented at the SPE International Symposium and Exhibition on Formation Damage Control, Lafayette, Louisiana, February 18-20, 2004.

3. Figueroa, J., Hibbeler, J., Duque, L. and Perdomo, L.: "Skin Damage Removal Using Coiled Tubing Vacuum: A Case Study in Venezuela's Orinoco Belt," SPE paper 69532, presented at the SPE Latin American and Caribbean Petroleum Engineering Conference, Buenos Aires, Argentina, March 25-28, 2001.

4. Hibbeler, J., Duque, L., Castro, L., Gonzalez, A., et al.: "Underbalanced Coiled Tubing Technique Leads to Improved Productivity in Slotted Liner Completions," SPE paper 74846, presented at the SPE/ICoTA Coiled Tubing Conference and Exhibition, Houston, Texas, April 9-10, 2002.

5. Clancy, T.F., Falk, K.L. and Duque, L.: "Concentric Coiled Tubing Well Vacuuming Technology for Complex Horizontal Wells in Eastern Venezuela," SPE paper 60696, presented at the SPE/ICoTA Coiled Tubing Roundtable, Houston, Texas, April 5-6, 2000.

6. Falk, K.L. and Fraser, B.: "Concentric Coiled Tubing Applications for Sand Cleanouts in Horizontal Wells," *Journal of Canadian Petroleum Technology*, Vol. 37, Issue 10, October 1998, pp. 46-50.

7. Heikkinen, B.K., Kuchel, M.P., Stang, Q.S., Misselbrook, J.G., et al.: "Drilling Damage Removal Using Multipoint Drawdown Along the Horizontal Wellbore," SPE paper 46011, presented at the SPE/ICoTA Coiled Tubing Roundtable, Houston, Texas, April 15-16, 1998.

8. Fried, S., Sudol, T. and Thornton, B.: "The Optimized Cleanup and Evaluation of Horizontal Wells Using Improved Jet Pump Technology," paper presented at the CADE/CAODC Spring Drilling Conference, Calgary, Alberta, Canada, April 8-10, 1997.

About the Authors

Hussain A. Almajid

B.S. in Petroleum Engineering, Louisiana State University

Hussain A. Almajid is a Production Engineer working in the Central Arabia Production Engineering Unit of Saudi Aramco's Southern Area Production Engineering Department. His work experience includes work in several oil fields, including Khurais, Central Arabia and in the North and South Ghawar fields. During this time, Hussain developed his experience as a skilled Technical Production Engineer dealing with intelligent field equipment, gas lift applications, electric submersible pumps, and smart well completions.

He has written and presented several Society of Petroleum Engineers (SPE) papers and presentations. Hussain is a certified SPE engineer.

In 2010, he received his B.S. degree in Petroleum Engineering from Louisiana State University, Baton Rouge, LA.

Alaa S. Shawly

B.S. in Petroleum Engineering, King Fahd University of Petroleum and Minerals

Alaa S. Shawly is a Supervisor of Production Engineering in the Central Arabia Production Engineering Unit in Saudi Aramco's Southern Area Production Engineering Department.

Prior to joining Saudi Aramco in 2006, he worked as a summer trainee with the Ain Dar and Shedgum Unit of the Reservoir Management Department for 8 weeks from July through August 2004. Alaa has 14 years of experience, mainly in acid stimulation and well intervention.

In 2006, he received his B.S. degree in Petroleum Engineering from King Fahd University of Petroleum and Minerals (KFUPM), Dhahran, Saudi Arabia.

Usman Ahmed

B.S. in Electronic Engineering, Ghulam Ishaq Khan Institute

Usman Ahmed started his career in 2007 in the oil and gas industry as a Well Services Engineer with Schlumberger. He has over 14 years of experience, focused primary on coiled tubing, stimulation, cementing technical and operational services, along with working transitionally in Account Management and Sales leadership roles.

Before joining Baker Hughes, Usman was the Well Intervention Technical Manger in National Petroleum Services Iraq.

He received his B.S. degree in Electronic Engineering from Ghulam Ishaq Khan Institute, Topi, Pakistan.